ENHANCED PERFORMANCES OF ORGANIC POLYMER SOLAR CELLS INCORPORATED WITH PLASMONIC NANOSTRUCTURES

THITIRAT PUTNIN

Doctoral Program in Electrical and Information Engineering
Graduate School of Science and Technology
Niigata University

ABSTRACT

Organic polymer solar cells (OPSCs) are promising candidates for renewable energy sources due to their advantages of low-cost solution process capability, flexibility, and scalable production. However, the power conversion efficiencies (PCEs) of OPSCs require the improvement of solar light utilization through light management. This strategy allows great enhancement of the light harvesting in OPSCs. Moreover, improving the light absorption in such OPSCs at a limited thickness of organic photoactive layer is challenging. There are two parts of the present research. Chapter II demonstrates the investigation of the effect of micro/nanoarchitectures or nanopatterns on the performances of OPSCs based on ITO/PEDOT:PSS/P3HT:PCBM/Al device configuration, and chapter III reports the investigation of dual plasmonic system introduced into the OPSCs in order to improve their light harvesting properties.

In Chapter II, the effect of imprinted nano/microstructures on the active layer (organic thin film) on performances of bulk-heterojunction (BHJ) OPSCs has been investigated and demonstrated. Patterned structures of the photoactive layer from compact disk recordable (CD-R), Blu-ray disk recordable (BD-R), nanodot, nanowell and honey comb were employed in this study. It was found that the nanostructures improved the light trapping in the OPSCs, which came up with higher PCE as compared to that of a bare device. The texture patterns acted as the diffraction structure for operating the induced strong diffusion and diffraction of incident light. The devices consisted of nano/microstructure-imprinted P3HT:PCBM and Al thin films. In comparison of the optical characteristics and the performances of pristine and imprinted BHJ OPSCs with a variety of the nano/microstructures, it was found that the nano/microstructures increased the short circuit current (I_{sc}), the fill factor (FF), %PCE and the cell performances. Moreover, the different types of the nano/microstructure affected the light tapping, which led to higher efficiencies due to the increased absorption, thus resulting in better current generation.

The best %PCE of 3.09 with highest improvement (24.09%) was observed for our OPSC imprinted with a BD-R grating (pitch size of 320 nm).

In Chapter III, we also studied the performance enhancement of OPSCs by introducing surface plasmon resonance (SPR) phenomena originated from grating-coupling technique and addition of plasmonic metallic nanoparticles (NPs) such as Au NPs, Ag NPs, Ag nanospheres (NSs) and a series of Ag nanodisks (NDs) into PEDOT:PSS hole transport layer (HTL). The device configuration designed was of grating-imprinted Al/P3HT:PCBM/metal NPs:PEDOT:PSS/ITO. The best device performances in terms of high current density, high charge mobility, and high PCE were found with dual plasmonic system based on both Al grating on device and Ag NDs incorporated into HTL. It was found that dual plasmonic device with Ag NDs (size of *ca*. 70 nm) revealed the best performances with %PCE of 3.59 and % improvement of 20.47. The results above indicated that the light absorption enhancement at the active layer was caused by SPR excitation with strong near-field distributions penetrated into absorption polymer and the broadband absorption enhancement in the rage of 350-800 nm leads to higher efficiencies, thus resulting in better current generation.

KEYWORDS: organic polymer solar cell, nanoimprinting, grating structure, nanostructure, Au nanoparticles, Ag nanoparticles, Ag nanodisks, dual plasmonic system

ACKHOWLEDGEMENTS

I would like to express my deeply gratitude to my supervisors, Associate Professor Dr. Akira Baba and Assistant Professor Dr. Kontad Ounnunkad, for their kind guidance and suggestion by all the ways through this research work. I would like to thank Professors Dr. Futao Kaneko, Dr. Keizo Kato, and Dr. Kazunari Shinbo, and Assistant Professor Dr. Chutiparn Lertvachirapaiboon from Niigata University for research comments and helps.

I would like to thank Dr. Supeera Nootchanart and Dr. Apichat Pangdam for helping me several techniques and sharing their happiness during my stay in Japan. I would like to thank to all members of Center for Transdisciplinary Research, Niigata University and our research laboratory, Chiang Mai University, for their assistance and encouragement.

Finally, I would like to dedicate this thesis dissertation to the memory of my parents, beloved family, and Mr. Wootichai Khotasen, who generously supported and encouraged me through the year of this study in Japan. Moreover, I would like to thank my aunt Miss Utumporn Malaithong for her unconditional love and support.

THITIRAT PUTNIN

August 2019

CONTENTS

LIST OF FIGURES

Page

Page

Page

Page

LIST OF TABLES

LIST OF ABBREVIATIONS

OPSCs	Organic polymer solar cells (thin film organic solar cells)
LSPR	Localized surface plasmon resonance
SP	Surface plasmon
GCSPP	Grating couple surface plasmon resonence
SPP	Surface plasmon polariton
HTM	Hole transporting material
HTL	Hole transport layer
ETL	Electron transport layer
LUMO	Lowest unoccupied molecular orbital
HOMO	Highest occupied molecular orbital
%PCE	Percent of Power Conversion Efficiency
FDTD	Finite-difference time-domain
IPCE	Incident photon to current efficiency
R_s	Series resistance
R_{sh}	Short resistance
R_{ct}	Charge transfer resistance
RMS	Root mean square
E.F.	Enhancement factor
J_{sc}	Short-circuit current density
V_{oc}	Open-circuit voltage
FF	Fill factor
P_m	Maximum power
J_m	Current density
V_m	Voltage

P_{in}	Incident photon power
NPs	Nanoparticles
Au NPs	Gold nanoparticles
Ag NSs	Silver nanospheres
Ag NDs	Silver nanodisks
P3HT	Poly(3-hexylthiophene)
PCBM	Phenyl-C_{61}-butyric acid methyl ester
PEDOT:PSS	Poly(3,4-ethylenedioxythiophene) polystyrene sulfonate
AFM	Atomic force microscope
TEM	Transmission electron microscope
SEM	Scanning electron microscope
UV-vis	Ultraviolet and visible
IPCE	Photo to current conversion efficienc

CHAPTER I

INTRODUCTION

1.1 ORGANIC POLYMER SOLAR CELLS

Organic polymer solar cells (OPSCs) are one type of photovoltaic cells that use organic electronics, for instance, conductive organic polymers or small organic molecules for light absorption and charge transport [1-3]. Various kinds of OPSCs have attracted considerable attention due to lightweight, flexible, and low temperature fabrication and can be produced inexpensively and suitable for mass production [4-5]. Polymer bulk-heterojunctions (BHJs) architecture is successfully designed for the polymeric photovoltaics. Excitons formed near a heterojunction are harvested near-perfect through a highly folded architecture [6-8]. Recently, the power conversion efficiency (PCE) of solar cells based on BHJs was reported to surpass 9-10% base on binary, ternary, or tandem structures. But their energy conversion efficiencies are significantly low at present, compared to other inorganic counterparts such as silicon and perovskite solar cells [9-10].

BHJs OPSCs generally consists of two components, i.e. donor and acceptor organic molecules. Usually, donor molecules are conjugate polymers, conjugate pigments or conducting oligomers such as MDMD-PPV, PPVFV, P3HT, PCPDTBT, F8T2, PDTSBT and PFDTBT. The acceptor materials are fullerene (C_{60}) and its derivatives such as PCBM-60, PCBM-70, mKMC60s, dMKC60s, bis-PCBM and modified PCBMs. The polymer donor and acceptor materials are shown in Figures 1.1 and 1.2, respectively. Actually, the principle of exciton operation in OPSCs can be described by level energy diagram. In BHJs OPSCs, donor materials act as a light absorber to absorb photon and acceptor materials act as an electron acceptor. Briefly, donor molecules absorb photon from the solar light and then electrons are excited from the highest occupied molecule orbital (HOMO) to lowest unoccupied molecular

orbital (LUMO). After that, the excitons (electron-hole pairs) are generated between donor and acceptor. Then, the excitons diffuse to the interfaces of donor-acceptor where there is sufficient potential energy drop to split these excitons into the free charge carriers. After splitting into free charge carriers, each carrier must be transported to the respective electrode through the bicontinuous interpenetrating pathway while avoiding recombination and trapping of charges [11-12].

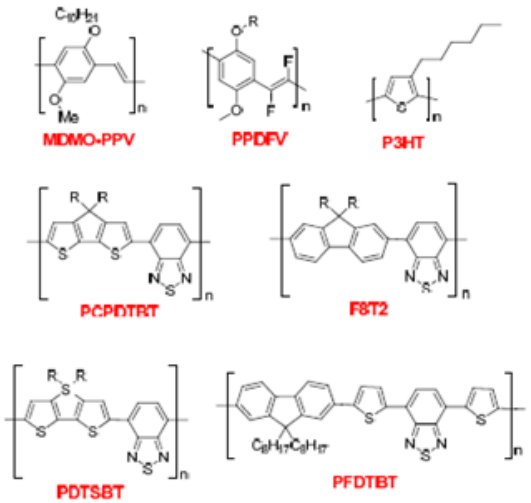

Figure 1.1 Chemical structures of some donor polymers used in BHJs solar cells [11].

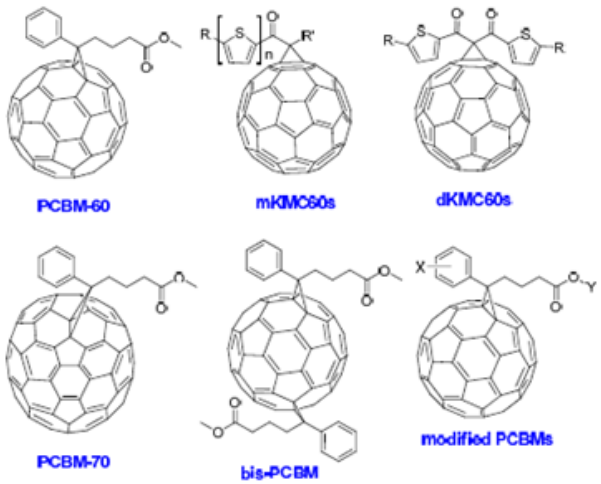

Figure 1.2 Chemical structures of some acceptor molecules used for BHJ solar cells [11].

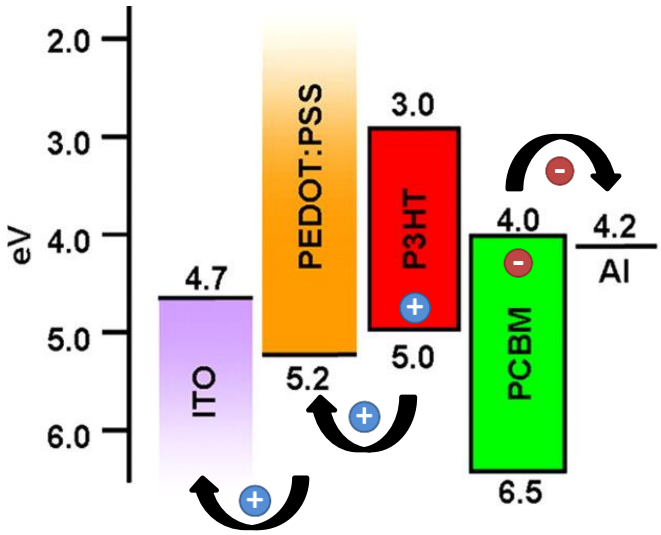

Figure 1.3 Electron energy level diagram of organic polymer solar cell [18].

In this work, we used P3HT donor polymer and PCBM acceptor to fabricate BHJs solar cells due to their commercial availability. P3HT exhibits a suitable solubility in organic solvents and chemical stability, a relatively low band gap (1.9-2.0 eV), and high hole mobility [13]. This polymer was blended with PCBM, which acts as the electron-acceptor material. This C_{60} derivatives has high solubility in common organic solvents [14]. P3HT is the most representative polymer donor with high hole mobility and ideal crystallization in the donor-acceptor (D-A) interpenetrating network of the active layer. P3HT has the HOMO energy level of 5.0 eV and LUMO energy level of 3.0 eV [15] while HOMO and LUMO energy levels of PCBM are equal to 6.5 eV and 4.0 eV, respectively. Moreover, the LUMO of hole-transporting material (HTM), poly(3,4-ethylenedioxythiophene):polystyrene sulfonate (PEDOT:PSS), is equal to 5.2 eV [16] which can induce a great moving of electron to anode and hole to cathode. To fabricate OPSCs, the P3HT/PCBM BHJs active layer is deposited on an indium-doped tin oxide (ITO) substrate coated with PEDOT:PSS layer and finally capped with aluminum metal (Al) as a metal back electrode and energy level diagram of OPSC as shown in Figure 1.3. This system possesses suitable energy levels for exciton dissociation. Although the maximum PCEs of P3HT/PCBM OPSCs are of ca. 4-5% [17], they can be improved by light management in

terms of maximized light harvesting using many strategies such as optimization of fabrication parameters and conditions, optimization of materials used, modification of materials, and use of plasmonic system.

Current-voltage (*I*-*V*) characteristic curves of the electrical devices or photovoltaic cells are a set of graphical curves, which are used to define their operation within an electrical circuit. Moreover, the *I*-*V* characteristic curves show the relationship between the current flowing through an electronic device and the applied voltage across its terminals as shown in Figure 1.4 [18-19].

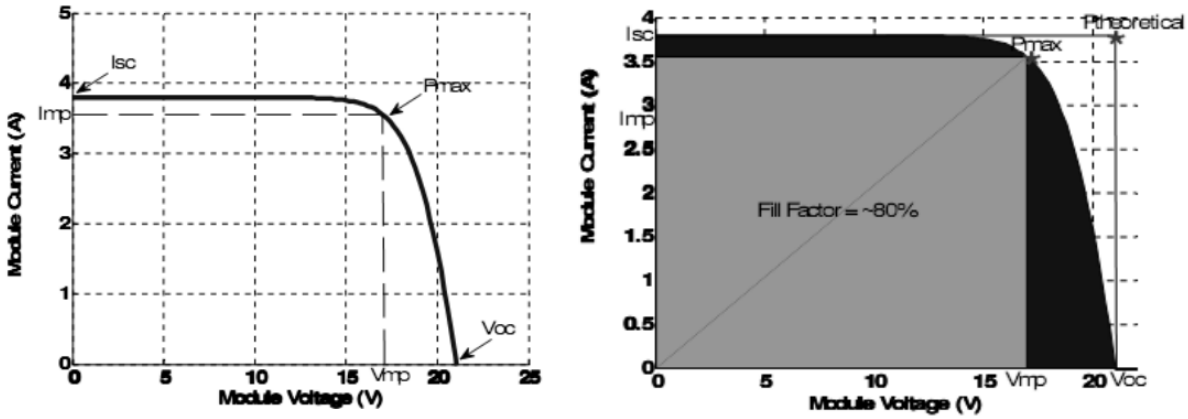

Figure 1.4 *I–V* characteristics of ideal solar cells [20].

According to Figure 4, several important parameters which are used to characterize solar cells such as open circuit voltage (V_{oc}), short circuit current (I_{sc}), fill factor (FF), and power conversion efficiency (PCE) are described as follows: V_{oc} value is the maximum voltage that the solar cell will supply and is the voltage without any load applied. I_{sc} is the maximum current of the solar under conditions of a zero resistance load, representing a free flow or zero volt potential drop across the cell. A FF parameter is the maximum power, showing how large the maximum power is in respect to the product of the V_{oc} and I_{sc}. The ratio between the

maximum power and the full square spanned by the V_{oc} and I_{sc} values. The FF value can be calculated as illustrated in equation (1).

$$FF = \frac{I_{mp}V_{mp}}{I_{sc}V_{oc}} \quad (1)$$

Where I_{mp} and V_{mp} are maximum point current and maximum point voltage values, respectively.

In addition, PCE is the ratio of generated electricity to incoming light energy. The calculation for the PCE is shown in equation (2).

$$PCE = \frac{I_{sc}V_{oc}FF}{P_{light}} \quad (2)$$

Where P_{light} is the power of incident light source (mW/cm^2)

1.2 INCREASE IN SOLAR CELLS PERFORMANCES BY LIGHT MANAGEMENT

As mention previously, the performance of OPSC is relatively low compared to that of inorganic photovoltaics [21-23]. Charge carrier mobility for most of the polymeric organic semiconductors is limited by the thickness of the organic active layer (<100 nm), which results in poor optical absorption [24-26]. Therefore, the enhancement of the absorbance of polymeric organic semiconductor with the specific limited thickness still remains a challenge. An alternative solution to the enhancement of the energy harvesting of the solar spectrum has been suggested, for example, textured surfaces, plasmonic nanoparticles (NPs), and grating-coupled surface plasmon resonance (GCSPR).

1.2.1 Textured Surfaces in Solar Cells

Modification of OPSCs with various kinds of textured surfaces can enhance the light collection and the effective optical path length of the light within absorber or photoactive layer [27-28]. Several research groups have reported a variety of random nanotextures and periodic nanostructures including nanopillars [29-30], nanorod [31-32], nanopencils [32-33], nanowells

[34-35], nanocones [36-37], nanodents [38-40], nanovoids [41-42] and nanogratings [43-44]. As aforementioned, it was found that the periodic nanostructures, namely nanopillas, nanorod, nanopencils and nanocones, have successfully reduced the Fresnel reflection [45] and led to directing and trapping more incident light into the OPSCs, thereby improving the short circuit current density and the PCE value, while another two nanostructures, i.e. nanowell, nanodents, and nanovoids, can enhance the conversion efficiency of the photovoltaic cells by coupling incident light into the absorber layer. Moreover, the grating structure that is one kind of the exceptional nanoarchitectures can improve the light absorption or light harvesting due to light scattering and GCSPR (see Section 1.2.3). Additionally, textured surface modification can induce polymer chain alignment, which can enhance charge carrier transport in conjugated polymers [46].

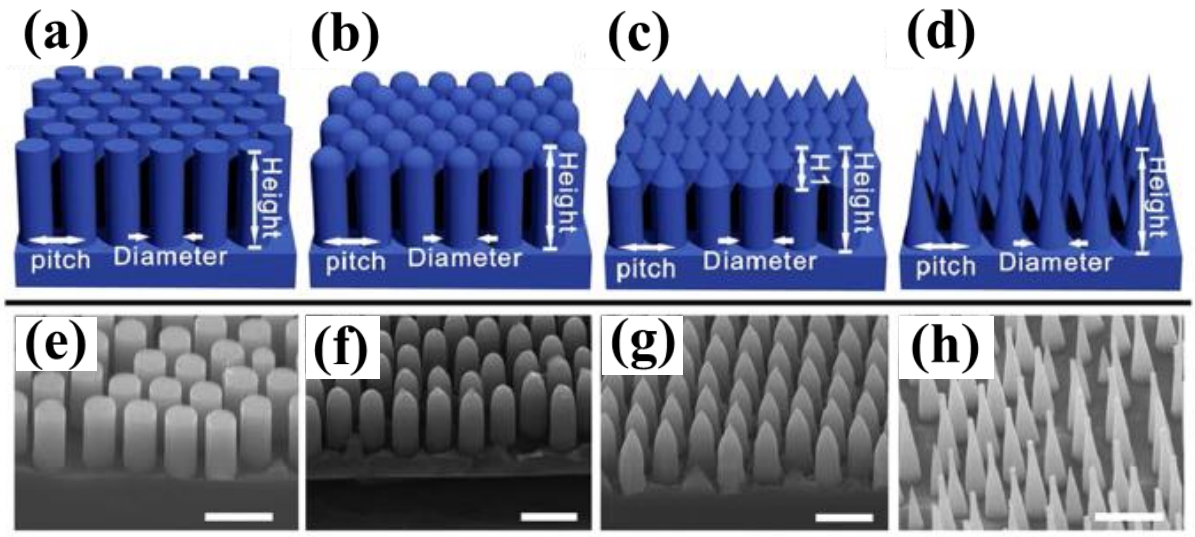

Figure 1.5 Illustration of nanostructures i.e (a) nanopillars, (b) nanorods, (c) inverted nanopencils, and (d) nanocones. The 45 tilted-angle-view SEM images of (e) nanopillars, (f) nanorods, (g) inverted nanopencils, and (h) nanocones. The structural pitches of all nanoarrays are 1.27 μm, and all scale bars are 2 μm [32].

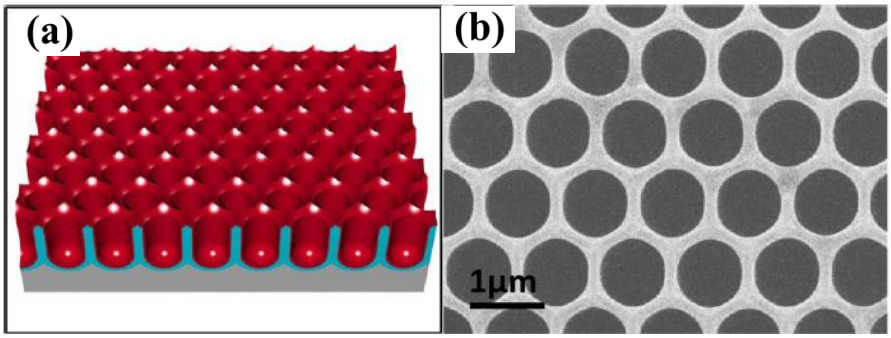

Figure 1.6 (a) Schematic drawing of ordered nanowells (NWLs) fabricated on Al substrate with red color representing conformal a-Si coating. (b) Top view SEM image of the 1 μm pitch NWL sample with NWL diameter widened to 870 nm [35].

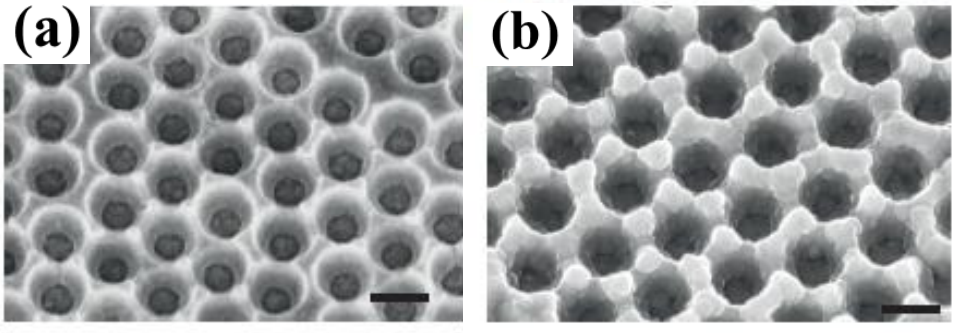

Figure 1.7 Schematic representation of substrate and layer structure. (a) Scanning electron micrographs of silver nanovoids (radius 250 nm) (b) nanovoids coated with 30 nm of Al:ZnO [42].

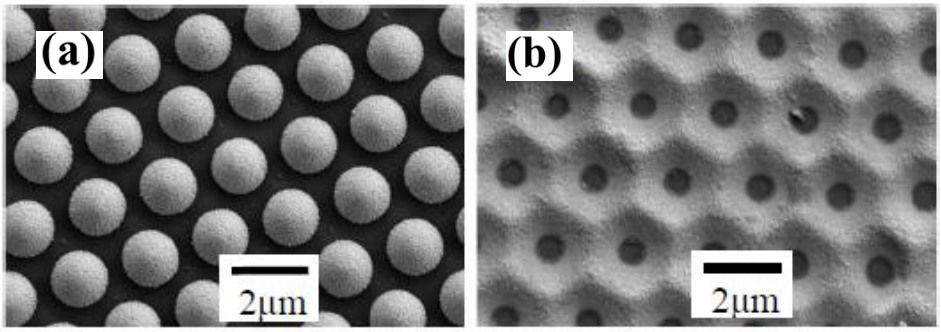

Figure 1.8 Top view SEM images of PS spheres reactively etched (a), and the resulting periodically hexagonal close-packed single-layer HZO films (b) [39].

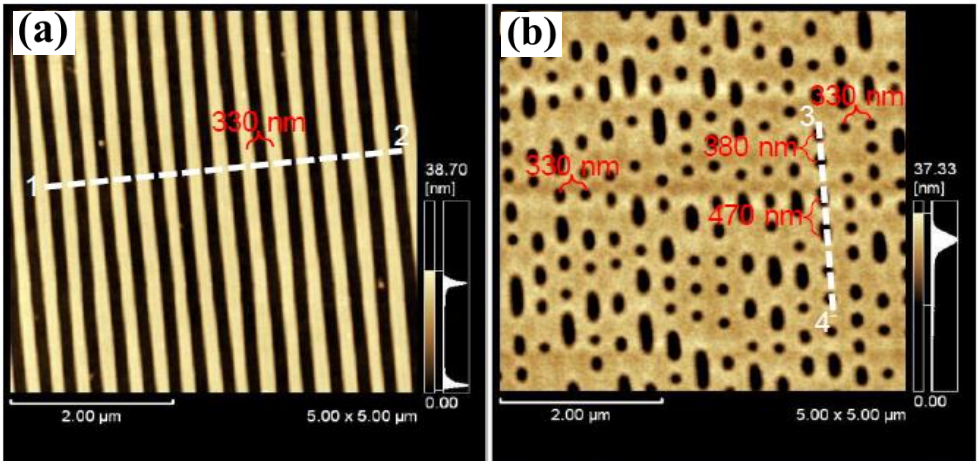

Figure 1.9 AFM images showing the surface morphology of grating structure (a) BD-R, and (b) BD [43].

1.2.2 Plasmonic Nanoparticles in Solar Cells

It has been growing interest in the uses of metallic nanoparticles (NPs), such as gold (Au) NPs or silver (Ag) NPs, in developing new OPSCs with higher efficiencies and device performances. Additions or blending of metal NPs in each OPSC component, for example in buffer layer, electron transport layer, hole transport layer, or active layer to achieve better PCE and light harvesting improvement of devices, were observed [26, 47-49]. The metal NPs are beneficial to better photoabsorption in OPSCs via localized surface plasmon resonance (LSPR) effect. LSPR phenomena of metal NPs occur by interaction between oscillating free electrons in the metal NPs and incident light. The LSPR of the metallic NPs not only scatter anisotropically but also absorb the incident light [50]. In addition, the easy tunability of the optical properties by modifying size, shape and surrounding materials of metal NPs has shown a high potential as an optical engineering tool in thin-film optoelectronic devices. Many research groups have reported the PCE enhancements of OPSCs by incorporating with metallic NPs, which are categorized as plasmonic OPSCs. In addition, PCE enhancement is related to the enhanced carrier effect and the exciton lifetime, conductivity, and the surface morphology of device element after modification with metal NPs [51-54].

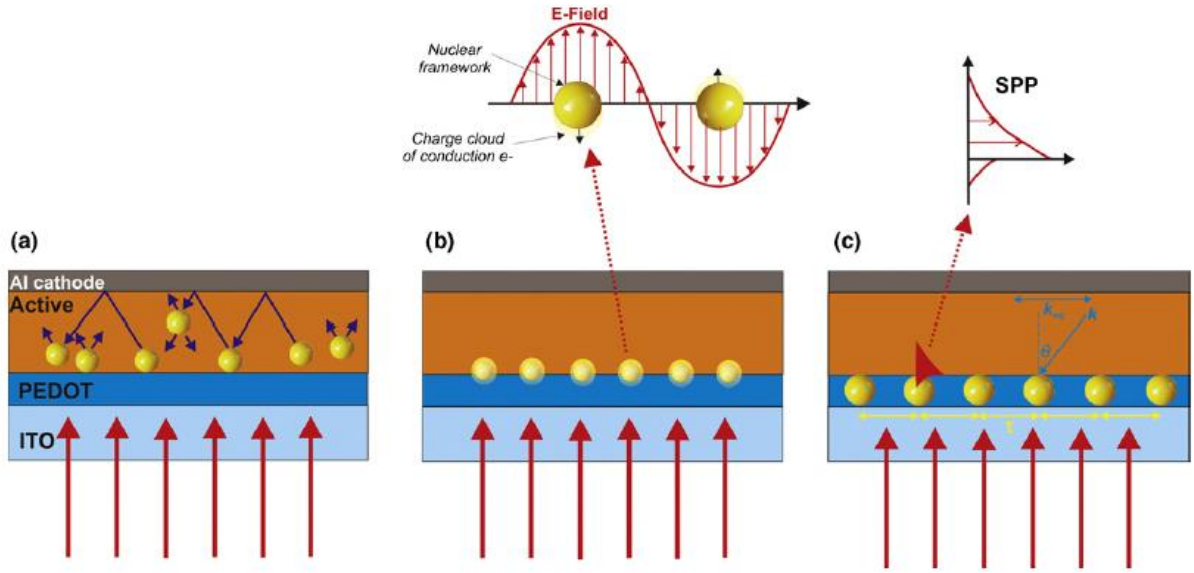

Figure 1.10 (Top) Schematic of the plasmon oscillation of a sphere, showing the displacement of the conduction electrons relative to the nuclei. (Bottom) Different geometries for plasmonic light trapping in OSC: (a) scattering from metal NPs into high angles inside the photoactive layer (b) LSPRs induced by metal particles and (c) excitation of SPPs at the NPs/photoactive layer interfaces [55].

Moreover, the metal NPs act as local field enhancers, light scattering centers or both, depending on their sizes. Small NPs with diameters in the range of 5-20 nm behave as subwavelength antennas, due to LSPR excitation (Figure 1.10(b)). The plasmonic near-field is directed to the photoactive layer, which can enhance its effective absorption cross-section and then improve exciton dissociation [56]. On the other hand, NPs with larger diameter (>50 nm) act as effective subwavelength scattering elements that govern freely propagating plane waves of the incident light into the photoactive layer (Figure 1.10(a)) [57]. At LSPR excitation, such NPs reveal a larger scattering cross-section as compared with their geometric cross-section. In this case, enhanced absorption occurs by an increase in the optical path length inside the photoactive layer, resulted from the light being reemitted in different directions within the photovoltaic cell. Furthermore, NPs can be put in the form of a periodically arranged nanoarray

at the front or back contact of the devices (Figure 1.10(c)). In this case, incident light can excite resonant scattering modes coined as surface plasmon polaritons (SPP) at each individual NP-active layer interface, which improve light adsorption ability as well as device performances. Depending on the NP shape, various modes can be excited, attributed to geometric resonances of SPPs at the NPs-layer interface [58].

1.2.3 Grating-coupled Surface Plasmon Resonance for Fabrication of Solar Cells

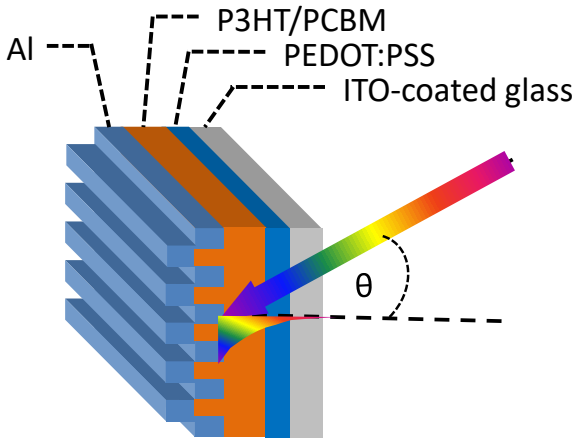

Figure 1.11 Device configuration of OPSCs fabricated on a metallic grating electrode.

Grating-coupled surface plasmon resonance (GCSPR) is a phenomenon of propagating surface plasmon (SP) excitation along grating-patterned metal surface. The grating-coupled technique is a prismless, convenient, propagating SPR excitation method [59-60] Light scattering and light trapping in OPSCs can be obtained on the grating surface (without SP excitation), resulting in the improvement of the obtained photocurrent [61]. In addition to the light scattering improvement effect, the photocurrent of the OPSCs can be remarkably improved via the SP-enhanced field on grating substrates. Recently, the fabrication of BHJ OPSCs on metallic grating having SP excitations efficiently improve the photocurrent conversion [62]. Moreover, the device configuration of SPR-enhanced OPSC is shown in Figure 1.11. The use of Al grating in the construction of OPSCs, in which governs the

excitation of grating-coupled SP and light scattering, benefits enhancement of their conversion efficiencies [63].

1.3 OBJECTIVES OF THE DISSERTATION

To develop and fabricate new plasmonic OPSCs, we employed the nanoimprint lithography (NIL) technique in creating highly periodic micro/nanostructures on active layer. The effect of architectures imprinted by selected patterns on properties and performances of our OPSCs was investigated. Moreover, in order to manage the light harvesting, we also employed plasmonic nanoparticles and imprinted plasmonic patterns via single and dual plasmonic systems in the construction of our OPSCs. To enhance light trapping for harvesting the broadband solar light, the metallic NPs involving Au and Ag NPs were used in incorporating into the hole-transporting PEDOT:PSS layer. The best light harvesting in our plasmonic OPSCs is expected to be achieved via our plasmonic architectures. The details of design, fabrication and characterization using surface modification and plasmonic properties of grating/nanostructured metallic electrodes and both metallic NPs for development of our OPSCs will be discussed later on. The main aims of this research project are:

1. To study the effect of different imprinted structures on the active layer of OPSCs.

2. To study the effect of metallic NPs blended into PEDOT/PSS hole-transporting layer (HTL) for improving the light harvesting of OPSCs.

3. To study the dual SPR phenomena originated from grating-coupled configuration and addition of Au and Ag NPs series into HTLs of our OPSCs for broadband light absorption.

1.4 SCOPE OF THE DISSERTATION

In this study, we investigated plasmonic architectures, including addition of metallic NPs and textured surface electrodes and grating structures on top electrodes by imprinting

technique, for construction of hybrid BHJs P3HT:PCBM OPSCs. First, textured surface and grating-structure top metallic electrodes, which were fabricated using micro/nanostructures such as compact disc recordable (CD-R), Blu-ray disc recordable (BD-R), nanowell arrays, nanodot arrays, and honeycomb structures, on OPSCs were investigated. The device performances and properties of OPSCs with such structures above were examined and the relation of the structures and our device properties will be discussed (see Chapter II). Incorporating metallic NPs into PEDOT:PSS buffer layers with/without the imprinted active layer with a BD-R pattern, which made grating structure on metallic electrode (Al electrode), was introduced in order to enhance the light harvesting in our OPSCs (see Chapter III). Two types of metallic NPs (Au NPs and Ag NPs) synthesized from a wet chemical reduction, which perform the strong light trapping, were blended into the PEDOT:PSS solution. The influences of NPs type and size in the PEDOT:PSS on the properties of the proposed OPSCs were studied using UV–visible spectroscopy and atomic force microscopy. In addition, to observe the plasmonic effects on the performances of the OPSCs, electrical characteristics of pristine and developed devices with our designed plasmonic metallic structures were analyzed from recorded *J*–*V* curves. The PCE value, improved performances and photocurrent enhancement in our developed OPSCs by employing different kinds of plasmonic systems and various sizes of metallic NPs in PEDOT:PSS HTL will be discussed. Regarding to this research work, there are two topics, which will be discussed in next two chapters. Chapter II shows the effect of micro/nanostructured P3HT:PCBM surfaces as different imprinted top Al electrodes on the performances of OPSCs while Chapter III represents the development of the dual plasmonic enhanced OPSCs by incorporating Au NPs or Ag NPs into HTL and patterning with grating-structure onto top Al electrode.

1.5 REFERENCES

[1] B. C. Thompson, J. M. J. Frechet, Polymer–fullerene composite solar cells, *Angewandte Chemie International ed. in English* **47[1]** (2008) 58-77.

[2] S. Gunes, H. Neugebauer, N. S. Sariciftci, Conjugated polymer-based organic solar cells, *Chemical Reviews* **107** (2007) 1324-1338.

[3] C. N. Hoth, P. Schilinsky, S. A. Choulis, C. J. Brabec, Printing highly efficient organic solar cells, *Nano Lette*r **8[9]** (2008) 2806-2813.

[4] T. D. Nielsen, C. Cruickshank, S. Foged, J. Thorsen, F. C. Krebs, Business, market and intellectual property analysis of polymer solar cells, *Solar Energy Materials and Solar Cells* **94** (2010) 1553-1571.

[5] Y. Liang, Z. Xu, J. Xia, S. T. Tsai, Y. Wu, G. Li, C. Ray, L. Yu, For the bright future-bulk heterojunction polymer solar cells with power conversion efficiency of 7.4%, *Advanced Materials* **22** (2010) 135-138.

[6] Z. He, C. Zhong, X. Huang, W. Y. Wong, H. B. Wu, L. W. Chen, S. J. Su, Y. Cao, Simultaneous enhancement of open-circuit voltage, short-circuit current density, and fill factor in polymer solar cells, *Advance Materials* **23** (2011) 4636-4643.

[7] C. E. Small, S. Chen, J. Subbiah, C. M. Amb, S. W. Tsang, T. H. Lai, J. R. Reynolds, F. So, High-efficiency inverted dithienogermole-thienopyrrolodione-based polymer solar cells, *Nature Photonics* **6** (2012) 115-120.

[8] L. Dou, J. B. You, J. Yang, C. C. Chen, Y. J. He, S. Murase, T. Moriarty, K. Emery, G. Li, and Y. Yang, Tandem polymer solar cells featuring a spectrally matched low-bandgap polymer, *Nature Photonics* **6** (2012) 180-185.

[9] Z. He, C. Zhong, S. Su, M. Xu, H. Wu, Y. Cao, Enhanced power-conversion efficiency in polymer solar cells using an inverted device structure. *Nature Photonics* **6** (2012) 591-595.

[10] S. W. Baek, J. Noh, C. H. Lee, B. S. Kim, M. K. S, J. Y. Lee, Plasmonic Forward Scattering Effect in Organic Solar Cells: A Powerful Optical Engineering Method, *Scientific Reports* **3[1726]** (2013) 1-7.

[11] S. Khanna, K. Khanna, G. Xavier, K. Prakhar, Plasmonic Study of Nanoparticles in Organic Photovoltic Cells: A Review, *Journal of Organic & Inorganic Chemistry* **3(1)** (2017) 1-8.

[12] D. S. Fung, C. H. Choy, Organic Solar Cells: Materials and Device Physics, Green Energy and Technology (2013) 1-266.

[13] D. H. Kim, Y. D. Park, Y. S. Jang, H. C. Yang, Y. H. Kim, J. I. Han, D. G. Moon, S. J. Park, T. Y. Chang, C. W. Chang, M. K. Joo, C. Y. Ryu, K. W. Cho, Enhancement of field-effect mobility due to surface-mediated molecular ordering in regioregular polythiophene thin film transistors, *Advanced Functional Materials* **15[1]** (2005) 77-82.

[14] M. R. Reyes, K. Kim, D. L. Carroll, High-efficiency photovoltaic devices based on annealed poly(3-hexylthiophene) and 1-(3-methoxycarbonyl)-propyl-1-phenyl-(6,6)C61 blends, *Applied Physics Letters* **87[8]** (2005) 083506(1)-083506(3).

[15] F. Xi, C. Chaohua, F. Guojia, W. Jinzhao, L. Songzhan, C. Fei, L. Hao, L. Yongfang, Efficient polymer solar cells based on poly(3-hexylthiophene):Indene-C70 bisadduct with a MoO_3 buffer layer, *Advanced Functional Materials* **22[3]** (2012) 585-590.

[16] L-C. Huang, H-W. Liu, T-R. Chou, J. Hsieh, W-Y. Chiu, L. Wang, C-Y. Chao, Patterning of Poly(3,4-Ethylenedioxythiophene):Poly(Styrenesulfonate) films via the rubbing

method in organic photovoltaic cells, *Journal of Physical Science and Application* **4[8]** (2014) 475-483.

[17] G. Li, V. Shrotriya, J. Huang, Y. Yao, T. Moriarty, K. Emery, Y. Yang, High-efficiency solution processable polymer photovoltaic cells by self-organization of polymer blends, *Nature Materials* **4** (2005) 864-868.

[18] M. D. Irwin, D. B. Buchholz, A. W. Hains, R. P. H. Chang, T. J. Marks, p-Type semiconducting nickel oxide as an efficiency-enhancing anode interfacial layer in polymer bulk-heterojunction solar cells, *Proceedings of the national academy of Sciences of the United States of America* **105[8]** (2008) 2783-2787.

[19] G. D. Spyropoulos, M. Stylianakis, E. Stratakis , E. Kymakis, Plasmonic organic photovoltaics doped with metal nanoparticles, *Photonics and Nanostructures-Fundamentals and Applications* **9** (2011) 184-189.

[20] PV EDUCATION.org [homepage on the Internet]. [Cited 2018 Dec 22]. Available from http://www.pveducation.org/pvcdrom/solar-cell-operation/iv-curve.

[21] M. M. Lee, J. Teuscher, T. Miyasaka, T. N. Murakami, H. J. Snaith, Efficient hybrid solar cells based on meso-superstructured organometal halide perovskites, *Science* **338** (2012) 643-647.

[22] N. J. Jeon, J. H. Noh, W. S. Yang, Y. C. Kim, S. Ryu, J. Seo, S. I. Seok, Compositional engineering of perovskite materials for high-performance solar cells, *Nature* **517[7535]** (2015) 476-480.

[23] M. A. Green, K. Emery, Y. Hishikawa, W. Warta, E. D. Dunlop, D. H. Levi, A. W. Y. Ho-Baillie, Solar cell efficiency tables (version 49), *Progress in Photovoltaics* **25[1]** (2017) 3-13.

[24] C. Deibel, V. Dyakonov, Polymer-fullerene bulk heterojunction solar cells, *Reports on Progress in Physics* **73** (2010) 096401(1)-096401(40).

[25] P. W. M. Blom, V. D. Mihailetchi, L. J. A. Koster, D. E. Markov, Device physics of polymer:fullerene bulk heterojunction solar cells, *Advance Materials* **19** (2007) 1551-1566.

[26] H. L. Gao, X. W. Zhang, Z. G. Yin, H. R. Tan, S. G. Zhang, J. H. Meng, and X. Liu, Plasmon enhanced polymer solar cells by spin-coating Au nanoparticles on indium-tinoxide Substrate, *Applied Physics Letters* **101** (2012) 133903(1)-133903(4).

[27] N. Tucher, H. Hausera, O. Höhna, V. Küblera, C. Wellensa, C. Müllerb, B. Bläsia, Interference and nanoimprint lithography for the patterning of large areas, *SPIE Conference Proceedings* **10115** (2017) 1011502(1)-1011502(7).

[28] H. Hauser, N. Tucher, K. Tokai, P. Schneider, C. Wellens, A. Volk, S. Seitz, J. Benick, S. Barke, F. Dimroth, C. Müller, T. Glinsner, B. Bläsia, Development of nanoimprint processes for photovoltaic applications, *Journal of Micro/Nanolithography, MEMS, and MOEMS* **14[3]** 031210(1)-031210(6).

[29] Z. Fan, R. Kapadia, P. W. Leu, X. Zhang, Y-L. Chueh, K. Takei, K. Yu, A. Jamshidi, A. A. Rathore, D. J. Ruebusch, M. Wu, A. Javey, Ordered Arrays of Dual-Diameter Nanopillars for Maximized Optical Absorption, *Nano Letters* **10** (2010) 3823-3827.

[30] Z. Fan, H, Razavi, J-W. Do, A. Moriwaki, O. Ergen, Y-L. Chueh, P. W. Leu, J. C. Ho1, T. Takahashi, L. A. Reichertz, S. Neale, K. Yu, M. Wu, J. W. Ager, A. Javey, Three-dimensional nanopillar-array photovoltaics on low-cost and flexible substrates, *Nature Materials* **8** (2009) 648-653.

[31] H. Jeong, H. Song, R. Lee, Y. Pak, Y. Kumaresan, H. Lee, G. Y. Jung, Orientation-controllable ZnO nanorod array using imprinting method for maximum light utilization in dye-sensitized solar cells, *Nanoscale Research Letters* **10[263]** (2015) 1-7.

[32] H. Lin, F. Xiu, M. Fang, S. P. Yip, H-Y. Cheung, F. Wang, N. Han, K. S. Chan, C-Y. Wong, J. C. Ho, Rational design of inverted nanopencil arrays for cost-effective, broadband, and omnidirectional light harvesting, *ACS Nano* **8[4]** (2014) 3752-3760.

[33] J. Chen, T. Subramani, W. Jevasuwan, K. Dai, K. Shinotsuka, Y. Hatta, N. Fukata, Fabrication of high-performance ordered radial junction silicon nanopencil solar cells by fine-tuning surface carrier recombination and structure morphology, *Nano Energy* **[56]** (2019) 604-611.

[34] C. Genet, T. W. Ebbesen, Light in tiny holes, *Nature* **445** (2007) 39-46.

[35] S. F. Leung, M. Yu, Q. Lin, K. Kwon, K. L. Ching, L. Gu, K. Yu, Z. Fan, Efficient photon capturing with ordered three-dimensional nanowell arrays, *Nano Letters* **12[7]** (2012) 3682-3689.

[36] S. Jeong, E. C. Garnett, S. Wang, Z. Yu, S. Fan, M. L. Brongersma, M. D. McGehee, Y. Cui, Hybrid silicon nanocone-polymer solar cells, *Nano Letters* **12[6]** (2012) 2971-2976.

[37] K-H. Tsui, Q. Lin, H. Chou, Q. Zhang, H. Fu, P. Qi, Z. Fan, Low-cost, flexible, and self-cleaning 3D nanocone anti-reflection films for high-efficiency photovoltaics, *Advance Materials* **26[18]** (2014) 2805-2811.

[38] H. Huang, L. Lu, J. Wang, J. Yang, S-F. Leung, Y. Wang, D. Chen, X. Chen, G. Shen, D. Li, Z. Fan, Performance enhancement of thin-film amorphous silicon solar cells with low cost nanodent plasmonic substrates, *Energy & Environmental Science*, **6** (2013) 2965-2971.

[39] B. Liu, X. Liang, J. Liang, L. Bai, H. Gao, Z. Chen, Y. Zhao, X. Zhang, Broadband light trapping based on periodically textured ZnO thin films, *Nanoscale* **7[21]** (2015) 9816-9824.

[40] C. Battaglia, K. Söderström, J. Escarré, F-J. Haug, D. Dominé, P. Cuony, M. Boccard, G. Bugnon, C. Denizot, M. Despeisse, A. Feltrin, C. Ballif, Efficient light management

scheme for thin film silicon solar cells via transparent random nanostructures fabricated by nanoimprinting, *Applied Physics Letters* **96** (2010) 213504(1)-213504(3).

[41] R. B. Dunbar, H. C. Hesse, D. S. Lembke, L. Schmidt-Mende, Light-trapping plasmonic nanovoid arrays, *Physical Review B* **85[3]** (2012) 035301(1)-035301(7).

[42] N. N. Lal, H. Zhou, M. Hawkeye, J. K. Sinha, P. N. Bartlett,G. A. J. Amaratunga, J. J. Baumberg, Using spacer layers to control metal and semiconductor absorption in ultrathin solar cells with plasmonic substrates, *Physical Review B* **85[24]** (2012) 245318(1)-245318(10).

[43] S. Nootchanat, A. Pangdam, R. Ishikawa, K. Wongraveeb, K. Shinbo, K. Kato, F. Kaneko, S. Ekgasitb, A. Baba, Grating-coupled surface plasmon resonance enhanced organic photovoltaic devices induced by Blu-ray disc recordable and Bluray disc grating structures, *Nanoscale* **9[15]** (2017) 4963-4971.

[44] K. Hara, C. Lertvachirapaiboon, R. Ishikawa, Y. Ohdaira, K. Shinbo, K. Kato, F. Kaneko, A. Baba, Inverted organic solar cells enhanced by grating coupled surface plasmons and waveguide modes, *Physical Chemistry Chemical Physics* **19[4]** (2016) 2791-2796.

[45] H. P. Wang, K. Y. Lai, Y. R. Lin, C. A. Lin, J. H. He, Periodic Si nanopillar arrays fabricated by colloidal lithography and catalytic etching for broadband and omnidirectional elimination of Fresnel reflection. *Langmuir* **26[15]** (2010) 12855-12858.

[46] K. Zhao, H. U. Khan, R. Li, Y. Su, A. Amassian, Entanglement of conjugated polymer chains influences molecular self-assembly and carrier transport, *Advanced Functional Materials* **23** (2013) 6024-6035.

[47] A. Singh, A. Dey, D. Das, P. K. Iyer, Combined influence of plasmonic metal nanoparticle and dual cathode buffer layer for highly efficient rrP3HT: PCBM based bulk heterojunction solar cell, *Journal of Materials Chemistry C* **5** (2017) 6578-6587.

[48] F. Otieno, N. P. Shumbula, M. Airo, M. Mbuso, N. Moloto, R. M. Erasmus, A. Quandt, D. Wamwangi, Improved efficiency of organic solar cells using Au NPs incorporated into PEDOT:PSS buffer layer, *AIP Advances* **7** (2017) 085302(1)-085302(10).

[49] M. Notarianni, K. Vernon, A. Chou, M. Aljada, J. Liu, N. Motta, Plasmonic effect of gold nanoparticles in organic solar cells, *Solar energy* **106** (2014) 23-37.

[50] J. Y. Lee, P. Peumans, The origin of enhanced optical absorption in solar cells with metal nanoparticles embedded in the active layer, *Optics Express* **18** (2010) 10078-10087.

[51] X. M. Lu, M. Rycenga, S. E. Skrabalak, B. Wiley, Y. N. Xia, Chemical synthesis of novel plasmonic nanoparticles, *Annual Review of Physical Chemistry* **60** (2009) 167-192.

[52] K. L. Kelly, E. Coronado, L. L. Zhao, G. C. Schatz, The optical properties of metal nanoparticles: The influence of size, shape, and dielectric environment, *Journal of Physical Chemistry B* **107** (2003), 668-677.

[53] E. Hutter, J. H. Fendler, Exploitation of localized surface plasmon resonance, *Advanced Materials*, **16** (2004) 1685-1706.

[54] F-C. Chen, J-L. Wu, C-L. Lee, Y. Hong, C-H. Kuo, Plasmonic-enhanced polymer photovoltaic devices incorporating solution-processable metal nanoparticles. *Applied Physics Letters* **95** (2009) 013305(1)-013305(3).

[55] E. Stratakis, E. Kymakis, Nanoparticle-based plasmonic organic photovoltaic devices, *Materials Today* **16[4]** (2013) 133-146.

[56] S. Pillai, K. R. Catchpole, T. Trupke, M. A. Green, Surface plasmon enhanced silicon solar cells, *Journal of Applied Physics* **101** (2007) 093105(1)-093105(8).

[57] C.F. Bohren, D.R. Huffman, Absorption and scattering of light by small particles, Wiley-Interscience, New York, 1983.

[58] F. J. Beck, E. Verhagen, S. Mokkapati, A. Polman, K. R. Catchpole, Resonant SPP modes supported by discrete metal nanoparticles on high-index substrates, *Optics Express* **19[S2]** (2011) A146-A156.

[59] J. Homola, I. Koudela, S. S. Yee, Surface plasmon resonance sensors based on diffraction gratings and prism couplers: sensitivity comparison, *Sensor and Actuators B* **54[1-2]** (1999) 16-24.

[60] B. K. Singh, A. C. Hillier, Surface plasmon resonance imaging of biomolecular interactions on a grating-based sensor array, *Analytical Chemistry* **78[6]** (2006) 2009-2018.

[61] L. Zeng, P. Bermel, Y. Yi, B. A. Alamariu, K. A. Broderick, J. Liu, C. Hong, X. Duan, J. Joannopoulos, L. C. Kimerling, Demonstration of enhanced absorption in thin film Si solar cells with textured photonic crystal back reflector, *Applied Physics Letters* **93[22]** (2008) 221105(1)-221105(3).

[62] A. Baba, K. Kanda, T. Ohno, Y. Ohdaira, K. Shinbo, K. Kato, F. Kaneko, Multimode surface plasmon excitations on organic thin film/eetallic diffraction grating, *Japanese Journal of Applied Physics* **49** (2010) 01AE02(1)-01AE02(4).

[63] A. Baba, N. Aoki, K. Shinbo, K. Kato, F. Kaneko, Grating-coupled surface plasmon enhanced short-circuit current in organic thin-film photovoltaic cells, *ACS Applied Materials & Interfaces* **3** (2011) 2080-2084.

CHAPTER II

EFFECT OF MICRO/NANOSTRUCTURED P3HT:PCBM SURFACES ON THE PERFORMANCE OF ORGANIC PHOTOVOLTAIC DEVICES

2.1 ABSTRACT

In this study, the effect of periodic patterned micro/nanostructures on the active layers of thin-film organic photovoltaics (OPVs) was investigated to improve the device performance. The patterned active layer structures were fabricated by a nanoimprinting technique using different templates, including compact disc recordable (CD-R), Blu-ray disc recordable (BD-R), nanowell arrays, nanodot arrays, and honeycomb structures. The OPVs consisted of Al/nanostructured P3HT:PCBM/PEDOT:PSS/ITO. Compared with a flat reference OPV, all the micro/nanostructured OPVs exhibited higher performances, originating from enhanced light absorption due to light scattering and surface plasmon excitation at the patterned Al/P3HT:PCBM interfaces.

2.2 INTRODUCTION

Thin-film organic photovoltaics (OPVs) are promising photovoltaic devices with distinctive advantages such as low cost and flexibility [1–3]. However, the photoelectric conversion efficiency (PCE) of OPVs is limited by their weak light absorption due to their thin active layers [4-5]. Although increasing the active layer thickness would increase the light absorption, this decreases the device performance by increasing its series resistance [6-7]. Thus, an important challenge is to increase the light absorption inside OPV devices while minimizing the active layer thickness. Efficient light-trapping strategies involving the use of both non-plasmonic and plasmonic micro/nanostructures have been introduced to improve the device performance [8-9]. This improved light trapping at a specific wavelength, charge generation, and charge extraction. Textured or rough surfaces fabricated at active layer/electrode interfaces in OPV devices could enhance absorption by diffuse scattering within the active layer [10–12]. Using periodic gratings in the OPVs could increase absorption by diffraction of light inside the active layer [13–15]. Furthermore, employing plasmonic NPs

could improve light absorption *via* scattering and localized surface plasmon resonance (LSPR) [16–19].

Subwavelength nanostructures were introduced into OPVs via several approaches. Nanoimprint lithography (NIL) is a well-known technique for creating highly periodic micro/nanostructures on OPV surfaces [20–21]. We reported the use of NIL to create patterns using Blu-ray disc recordable (BD-R) and Blu-ray disc (BD) gratings on the surfaces of OPV active layers [22]. The OPV performance was improved by grating-coupled surface plasmon resonance (GCSPR), which induced additional light absorption at 600–800 nm. Furthermore, we employed a pattern created with a DVD-R grating to improve the photovoltaic performance in inverted OPVs using simultaneous GCSPR excitation and grating-coupled waveguide modes on gold grating surfaces [23]. Lal et al. [24] also reported a new class of plasmon-enhanced photovoltaics, in which the absorption was enhanced with nanovoid structures. As mentioned above, NIL is a versatile and efficient technique for creating highly homogeneous micro/nanostructures [25–27]. Additionally, it was found that charge carrier transport in conjugated polymers could be enhanced by NIL-induced polymer chain alignment [28–30]. Although several groups have used different types of micro/nanostructures in OPVs to improve the device performance, the detailed study of the effects of these structures on the optical and electrical characteristics of OPVs remains an interesting topic.

In this work, we study the effect of micro/nanostructures on OPV performances. Patterns of periodic micro/nanostructures, including compact disc recordable (CD-R), BD-R, nanodot arrays, nanowell arrays, and honeycomb, were transferred to active layer surfaces, which comprised a mixture of poly(3-hexylthiophene-2,5-diyl) (P3HT) and [6,6]-phenyl C61 butyric acid methyl ester (PCBM), by NIL. The optical and electrical properties of fabricated devices were studied systematically. The influence of periodic micro/nanostructures on the OPV performance was evaluated compared with reference (flat) devices.

2.3 EXPERIMENTAL

2.3.1 Preparation of PDMS replicas

Micro/nano structures were transferred from master templates to the active layers of OPVs using polydimethylsiloxane (PDMS) replicas. To prepare PDMS molds with negative patterns, a mixture of PDMS (Sylgard® 184) and its curing agent with a weight ratio of 10:1 was cast on cleaned master templates before removing air bubbles in a vacuum chamber for 3 h. Curing was then performed at 70°C for a further 3 h. After cooling to room temperature, the master template was detached from the PDMS replica as illustrated in Figure 2.1.

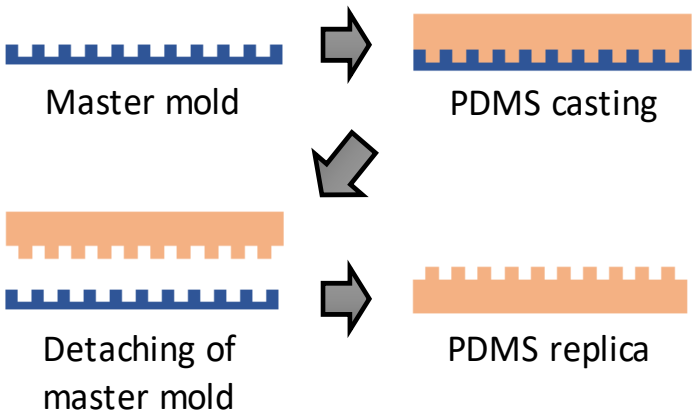

Figure 2.1. A schematic illustration of PDMS replica preparation from a master mold.

2.3.2 Fabrication of OPVs with micro/nano pattern back electrode

To fabricate OPV devices, a patterned indium tin oxide (ITO) coated glass was treated with UV/O_3 for 45 min before depositing a hole transport layer (Clevios^{TM} HTL Solar) by spin-coating at 3,000 rpm. After drying the hole transport layer at 120°C for 10 min in a vacuum chamber, the active layer, a mixture of P3HT:PCBM (weight ratio 1:0.8, 27 mg/ml in 1, 2-dichlorobenzene), was deposited on the hole transport layer by a two-step spin-coating method (1,500 rpm for 15 sec then 2,000 rpm for 45 sec), forming a homogeneous film with a thickness of ~100 nm. NIL was used to create nano/micro structures on the surface of the active layer as

shown in Figure 2.2(A). The PDMS replica with a negative pattern of micro/nano structures was carefully attached to active layer surfaces before annealing at 100°C in a vacuum chamber for 60 min. After cooling to room temperature, the PDMS replica was detached, and an aluminum top electrode was deposited. Post annealing was conducted at 150°C for 45 min before electrical characterization. The complete structures of fabricated OPVs with patterned back electrodes are shown in Figure 2.2(B).

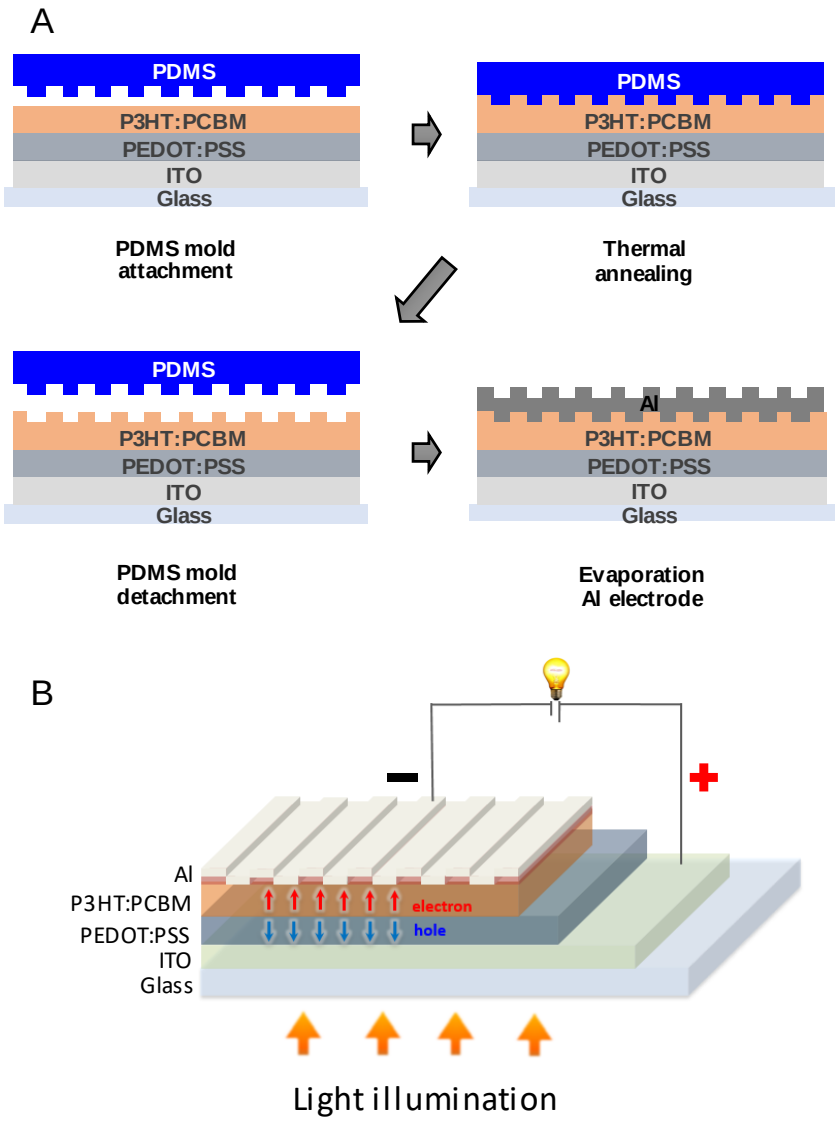

Figure 2.2 (A) Schematic illustrating the fabrication of OPVs with a grating back electrode using NIL. (B) Structure of fabricated OPV with metal grating electrode.

2.3.3 Characterization

The electrical characterization of fabricated OPVs was performed using an electrometer (B2901A, Agilent) or high-performance potentiostat (PARSTAT 4000, Princeton Applied Research) under illumination from a solar simulator (HAL-C100, Asahi Spectra). The surface morphologies of the fabricated devices were observed by atomic force microscopy (SPM-9600, Shimadzu). The optical properties of fabricated OPVs were characterized using an UV–Vis spectrometer (USB 4000, Ocean Optics).

2.4 RESULTS AND DISCUSSION

To fabricate patterns on the surfaces of OPV active layers, we performed NIL. Additionally, to achieve good quality imprinted patterns, NIL must be performed on damp polymer film. The residual solvent left in the film is important in helping the polymer to flow into the grooves of the PDMS replica during annealing above the glass transition temperature (T_g). The PCBM content in the P3HT:PCBM blend in this system is 45% w/w. The T_g of the blend is approximately 25°C [31]. Thus, annealing at 100°C during NIL is appropriate. Figure 2.3 shows AFM images of master templates used to create PDMS replicas. The master templates can be classified into two groups: one-dimensional (1D) and two-dimensional (2D) gratings. In the 1D grating group, the CD-R and BD-R gratings provide the same grating geometry, which is a periodic straight line, with different grating heights and pitches. For CD-R, Figure 2.3(A) shows that the height and pitch are 135 and 1,600 nm, respectively. For the BD-R, the grating height and pitch are 39 and 320 nm, respectively, as shown in Figure 2.3(B). In the 2D grating group, highly periodic nanowell arrays are clearly observed, as shown in Figure 2.3(C). The nanowell diameter is 250 nm with a depth of 30 nm. The nanodot arrays (Figure 2.3(D)) offer highly homogeneous half-spherical knotted patterns. The height and pitch of the nanodot structure were 250 and 50 nm, respectively. For honeycomb structures, Figure

2.3(E) exhibits hexagonal pillars with a diagonal distance and height of 730 and 150 nm, respectively.

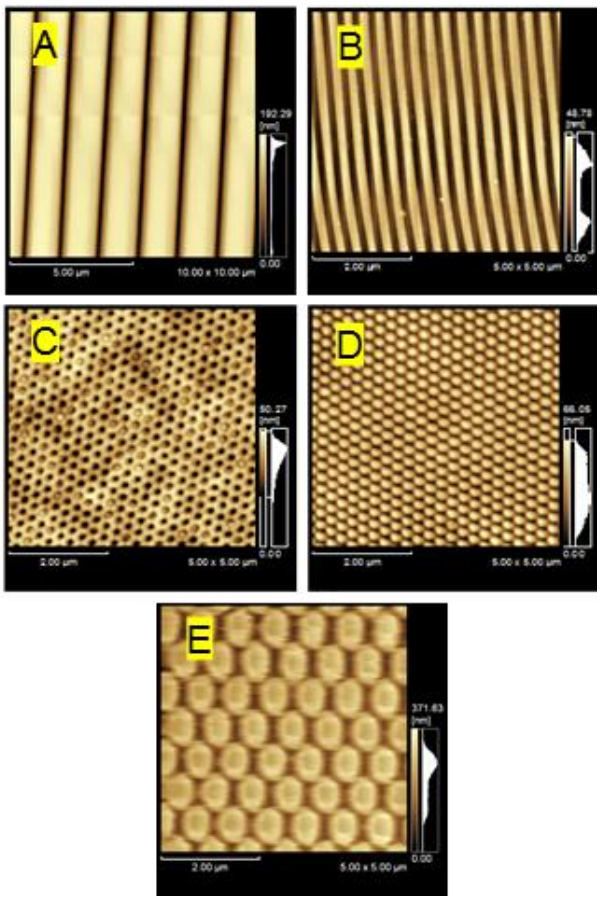

Figure 2.3 AFM images of master molds containing different micro/nano structures (A) CD-R, (B) BD-R, (C) nanowells, (D) nanodots, and (E) honeycomb.

Patterns were transferred from master templates to the surfaces of active layers using NIL. After evaporating aluminum from the patterned surfaces, complete OPVs with patterned back electrodes were obtained. Figure 2.4 shows AFM images of the aluminum surfaces of fabricated OPVs. These clearly show that the patterns of micro/nanostructures were fabricated on the surfaces of the OPV back electrodes. For all the micro/nanostructured devices, the heights of the patterns were lower than those of the templates. We found that NIL produced flawless 1D grating patterns. However, some defects were observed in the 2D grating. This

might be due to complexation of the structures themselves and to small air bubbles trapped in the complex structures of PDMS replicas.

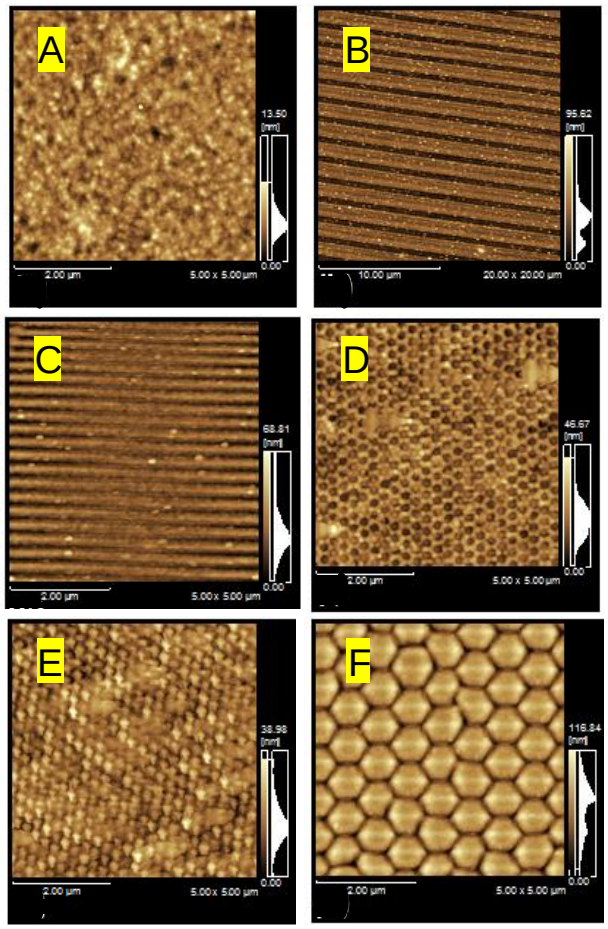

Figure 2.4 AFM images of the surface morphology of aluminum back electrodes of (A) Flat, (B) CD-R, (C) BD-R, (D) nanowell, (E) nanodot, and (F) honeycomb OPVs.

The performance of the fabricated devices was studied under illumination with unpolarized light. Figure 2.5 and Table 2.1 show the J-V properties and electrical parameters of OPV devices. The results clearly show improvements in J_{sc} and PCE for all patterned devices with insignificant modification of V_{oc}. For devices with 1D gratings, increases in J_{sc} from 5.62 to 5.93 and 7.10 mA/cm^2 were obtained for CD-R and BD-R structured devices, respectively, compared with the flat reference OPV. Increases in the PCE from 2.49% to 2.73% and 3.09% were also achieved in devices with CD-R and BD-R structures, respectively. For the 2D grating

structured devices, J_{sc} increased from 5.62 to 6.58, 6.15, and 6.71 mA/cm^2 for nanowells, nanodots, and honeycomb structured devices, respectively, compared with the flat reference OPV. Furthermore, increases in PCE from 2.49% to 2.65%, 2.50%, and 2.58% were obtained for devices with nanowells, nanodots, and honeycomb, respectively. However, a decrease in *FF* for the patterned devices was observed except with the CD-R device. It is known that the imprinting process aligns and organizes the polymer chains in the blended P3HT:PCBM active layers of OPVs [32–34], which enhances *FF*. However, among all the patterned OPVs, only the CD-R device showed an increase in *FF* from 0.54 to 0.56. Thus, imprinting-induced polymer chain alignment should not be the key parameter in improving the OPVs in our system. Although the patterned devices except CD-R showed a decrease in *FF*, the overall performance of the patterned devices was higher than that of the flat device.

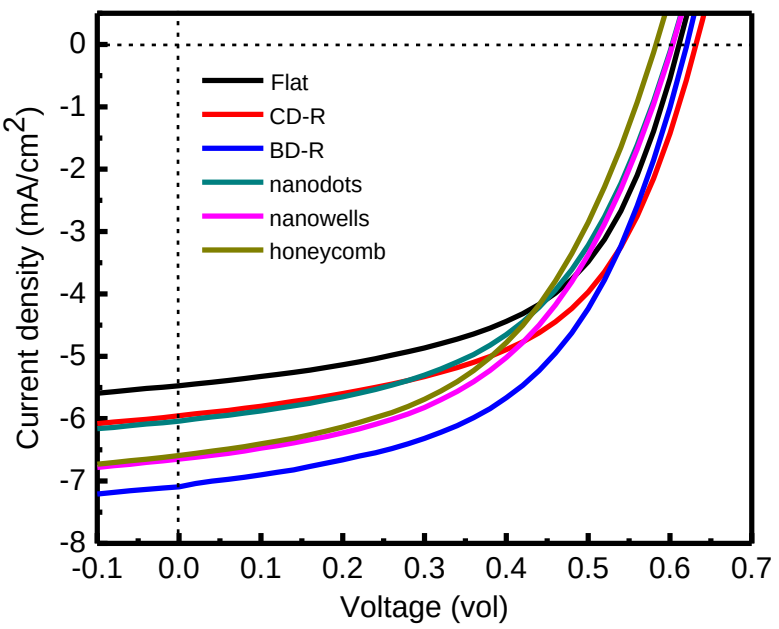

Figure 2.5 *J–V* characteristics of fabricated OPVs under illumination with unpolarized light with an intensity of 75 mW/cm^2.

Table 2.2 Electrical parameters of fabricated OPVs obtained from J-V characterization.

Devices	Pitch (nm)	Jsc (mA/cm^2)	V_{oc} (V)	FF	PCE (%)
Flat cell	-	5.62	0.61	0.54	2.49
CD-R	1600	5.93	0.62	0.56	2.73
BD-R	320	7.10	0.62	0.52	3.09
Nanodots	250	6.15	0.60	0.51	2.50
Nanowells	250	6.58	0.60	0.51	2.65
Honeycomb	730	6.71	0.59	0.49	2.58

As previously mentioned, we demonstrated that introducing grating structures into back electrodes of OPVs could enhance the device performance, which was mostly due to an increase in J_{sc}. To gain a better understanding of the performance enhancement, we studied the optical properties of the fabricated solar cells by conducting reflection measurements at incident light angles of 20°–50° under illumination with polarized light from the ITO/glass substrate side. Figure 2.6 shows the reflection spectra of the fabricated devices. A broadband absorption from 400–650 nm was clearly observed in all devices and attributed to the absorption characteristics of the P3HT:PCBM blended polymers. For the 1D grating, shown in Figure 2.6(B) and (C), we observed an improvement in the light absorption in the range 400–650 nm. This could be due to light scattering, which increased the effective distance traveled by light inside the active layer. Moreover, when the polarization of the incident light was changed from s- (s-pol) to p-polarization (p-pol), additional absorption dips originating from GCSPR were clearly observed [22, 35]. The GCSPR dips gradually shifted to longer wavelengths when the incident angle increased. These results indicate that the improvement in J_{sc} in the devices with CD-R and BD-R back electrodes originated from the improvement in light absorption due to light scattering and GCSPR.

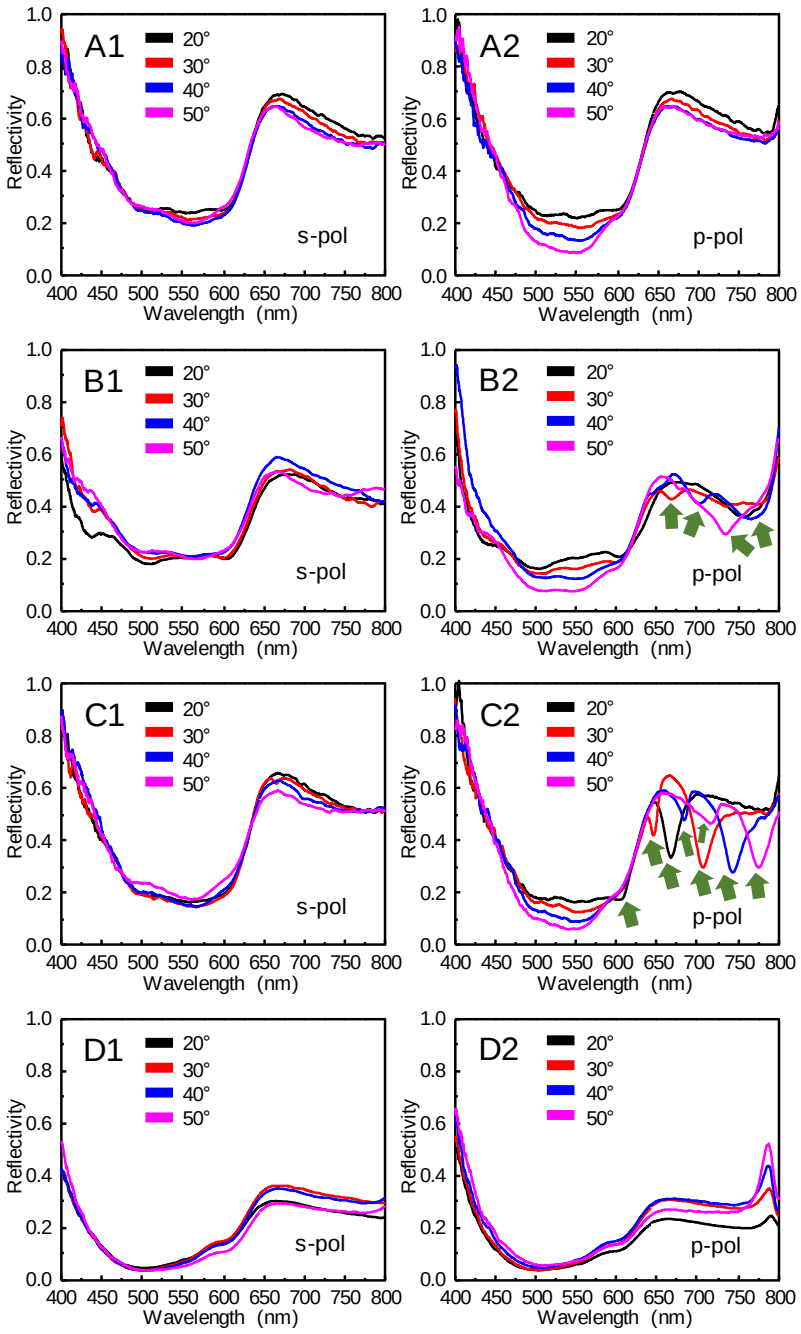

Figure 2.6 Reflectivity curves of (A) flat, (B) CD-R, (C) BD-R, (D) nanodot, (E) nanowell, and (F) honeycomb devices collected from transparent electrode side under illumination by (1) s- and (2) p-polarized light. Green arrows indicate plasmon excitation dips.

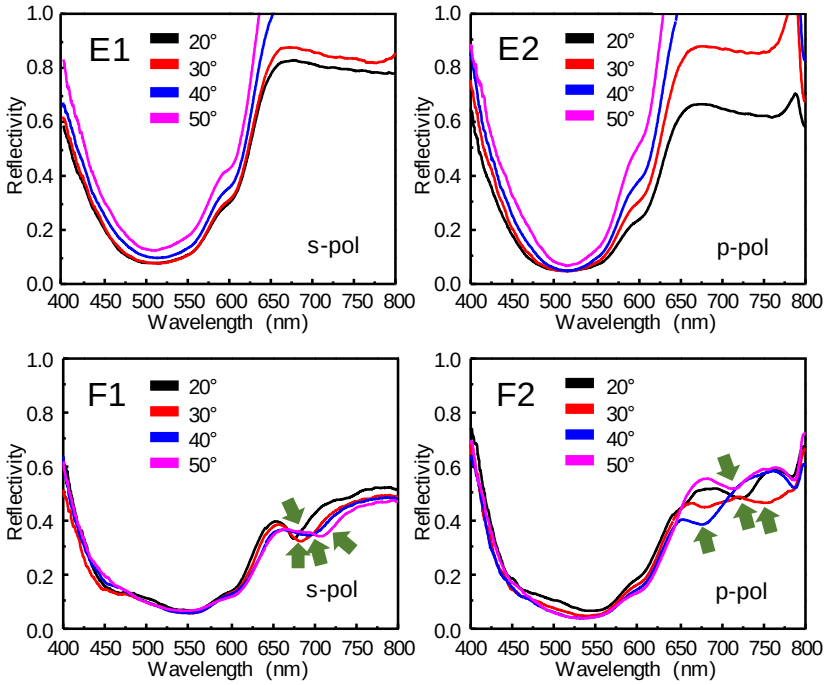

Figure 2.6 Reflectivity curves of (A) flat, (B) CD-R, (C) BD-R, (D) nanodot, (E) nanowell, and (F) honeycomb devices collected from transparent electrode side under illumination by (1) s- and (2) p-polarized light. Green arrows indicate plasmon excitation dips. (continued)

As shown in Figure 2.6(D)-(F), an improvement in light absorption from 400–650 nm was observed in all OPVs with 2D gratings. However, additional dips from GCSPR excitation were observed only for the honeycomb structures (Figure 2.6(F)). It is noteworthy that the honeycomb structures induced GCSPR excitation under both s-pol and p-pol illumination, as GCSPR dips were observed for both forms of polarization. A red-shift was observed in the GCSPR dips for the devices with honeycomb structures. Due to both the light scattering and GCSPR effects, J_{sc} was significantly increased compared with other 2D grating structures. However, *FF* decreased in this case, which might be due to the relatively large 2D grating height shown in Figure 2.4(F). However, the improvements in the OPV performances in nanodots and nanowells were obtained mainly from light scattering, because no GCSPR dips were observed. Additionally, defects observed in the AFM image, especially in nanodot structures, might

slightly improve the OPV device. Hence, we conclude that significant improvement of OPVs can be obtained from light scattering and GCSPR for non-defective micro/nanostructures.

2.5 CONCLUSIONS

We fabricated thin-film OPVs with grating back electrodes using NIL. Periodic 1D and 2D grating structures were completely transferred to the active layer of OPVs using PDMS replicas. Improvement of the OPV performance of the patterned devices was clearly observed. The improvement in the device performance originated mainly from an increase in light absorption, which was attributed to the effects of light scattering and GCSPR. The 1D gratings (CD-R and BD-R) could provide enhancement by both light scattering and GCSPR. For 2D gratings, the improvement in light absorption in nanodots and nanowells originated from light scattering, while the honeycomb structure provided both light scattering and GCSPR.

2.6 REFERENCES

[1] Y. Yang, K. Mielczarek, M. Aryal, A. Zakhidov, W. Hu, Nanoimprinted polymer solar cell, *ACS Nano* **6[4]** (2012) 2877-2892.

[2] L. T. Dou, Y. S. Liu, Z. R. Hong, G. Li, Y. Yang, Low-bandgap near-IR conjugated polymers/molecules for organic electronics, *Chemical Reviews* **115[23]** (2015) 12633-12665.

[3] K. Zhang, Z. Hu, C. Sun, Z. Wu, F. Huang, Y. Cao, Toward solution-processed high-performance polymer solar cells: from material design to device engineering, *Chemistry of Materials* **29[1]** (2017) 141-148.

[4] J. Yang, F. Luo, T. S. Kao, X. Li, G. W. Ho, J. Teng, X. Luo, M. Hong, Design and fabrication of broadband ultralow reflectivity black Si surfaces by laser micro/nanoprocessing, *Light: Science & Applications* **3[1]** (2014) e185-e192.

[5] S. H. Park, A. Roy, S. Beaupre, S. Cho, N. Coates, J. S. Moon, D. Moses, M. Leclerc, K.

Lee, A. J. Heeger, Bulk heterojunction solar cells with internal quantum efficiency approaching 100%, *Nature Photonics* **3[1]** (2009) 297-302.

[6] E. Stratakis, E. Kymakis, Nanoparticle-based plasmonic organic photovoltaic devices, *Materials Today* **16[4]** (2013) 133-146.

[7] A. Guerrero, T. Ripolles-Sanchis, P. P. Boix, G. Garcia-Belmonte, Series resistance in organic bulk-heterojunction solar devices: Modulating carrier transport with fullerene electron traps, *Organic Electronics* **13[11]** (2012) 2326-2332.

[8] Z. Tang, W. Tress, O. Inganäs, Light trapping in thin film organic solar cells, *Materials Today* **17[8]** (2014) 389-396.

[9] C. H. Chou, F. C. Chen, Plasmonic nanostructures for light trapping in organic photovoltaic devices, *Nanoscale* **6[15]** (2014) 8444-8458.

[10] J. Yun, W. Wang, S. M. Kim, T. S. Bae, S. Lee, D. Kim, G. H. Lee, H. S. Lee, M. Song, Light trapping in bendable organic solar cells using silica nanoparticle arrays, *Energy Environmental Science* **8[3]** (2014) 932-940.

[11] C. Cho, H. Kim, S. Jeong, S. W. Baek, J. W. Seo, D. Han, K. Kim, Y. Park, S. Yoo, J. Y. Lee, Random and V-groove texturing for efficient light trapping in organic photovoltaic cells, *Solar Energy Materials and Solar Cells* **115[1]** (2013) 36-41.

[12] B. Wang, T. Gao, P. W. Leu, Broadband light absorption enhancement in ultrathin film crystalline silicon solar cells with high index of refraction nanosphere arrays, *Nano Energy* **19[1]** (2016) 471-475.

[13] R. M. de Oliveira Hansen, Y. Liu, M. Madsen, H. G. Rubahn, Flexible PCPDTBT:PCBM solar cells with integrated grating structures, *SPIE - the international society for optics and photonics XIV* **8830[1]** (2013) 883021-1-883021-7.

[14] X. H. Li, W. E .I. Sha, W. C. H. Choy, D. D. S. Fung, F. X. Xie, Efficient inverted polymer solar cells with directly patterned active layer and silver back grating, *The Journal of*

Physical Chemistry C **116[12]** (2012) 7200-7206.

[15] S. I. Na, S. S. Kim, J. Jo, S. H. Oh, J. Kim, D. Y. Kim, Efficient polymer solar cells with surface relief gratings fabricated by simple soft lithography, *Advanced Functional Materials* **18[24]** (2008) 3956-3963.

[16] K. R. Catchpole, A. Polman, Plasmonic solar cells, *Optics Express* **16[22]** (2008) 21793-21800.

[17] V. E. Ferry, J. N. Munday, H. A. Atwater, Design considerations for plasmonic photovoltaics, *Advance Materials* **22[43]** (2010) 4794-4808.

[18] D. Duche, P. Torchio, L. Escoubas, F. Monestier, J. J. Simon, F. Flory, G. Mathian, Improving light absorption in organic solar cells by plasmonic contribution, *Solar Energy Materials and Solar Cells* **93[8]** (2009) 1377-1382.

[19] S. W. Baek, J. Noh, C. H. Lee, B. S. Kim, M. K. Seo, J. Y. Lee, Plasmonic forward scattering effect in organic solar cells: A powerful optical engineering method, *Scientific Reports* **3[1726]** (2013) 1-7.

[20] J-T. Chen, C-S. Hsu, Conjugated polymer nanostructures for organic solar cell applications, *Polymer Chemistry* **2[12]** (2011) 2707-2722.

[21] J. Weickert, R. B. Dunbar, H. C. Hesse, W. Wiedemann, L. Schmidt-Mende, Nanostructured organic and hybrid solar cells, *Advance Materials* **23[16]** (2011) 1810-1828.

[22] S. Nootchanat, A. Pangdam, R. Ishikawa, K. Wongraveeb, K. Shinbo, K. Kato, F. Kaneko, S. Ekgasitb, A. Baba, Grating-coupled surface plasmon resonance enhanced organic photovoltaic devices induced by Blu-ray disc recordable and Bluray disc grating structures, *Nanoscale* **9[15]** (2017) 4963-4971.

[23] K. Hara, C. Lertvachirapaiboon, R. Ishikawa, Y. Ohdaira, K. Shinbo, K. Kato, F. Kaneko, A. Baba, Inverted organic solar cells enhanced by grating coupled surface plasmons and

waveguide modes, *Physical Chemistry* **19[4]** (2016) 2791-2796.

[24] N. N. Lal, B. F. Soares, J. K. Sinha, F. Huang, S. Mahajan, P. N. Bartlett, N. C. Greenham, J. J. Baumberg, Enhancing solar cells with localized plasmons in nanovoids, *Optics Express* **19[12]** (2011) 11256-11263.

[25] H. Hauser, N. Tucher, K. Tokai, P. Schneider, C. Wellens, A. Volk, S. Seitz, J. Benick, S. Barke, F. Dimroth, C. Müller, T. Glinsner, B. Bläsi, Development of nanoimprint processes for photovoltaic applications, *Journal of Micro/Nanolithography, MEMS, and MOEMS* **14[3]** (2015) 1-6.

[26] N. Tucher, H. Hauser, O. Höhn, V. Kübler, C. Wellens, C. Müller, B. Bläsi, Interference and nanoimprint lithography for the patterning of large areas, *Proceedings of SPIE* **10115[1]** (2017) 1-7.

[27] L. J. Guo, Recent progress in nanoimprint technology and its applications, *Journal of Physics D: Applied Physics* **37[1]** (2004) R123-R141.

[28] Z. Zheng, K.-H. Yim, M. S. M. Saifullah, M. E. Welland, R. H. Friend, J.-S. Kim, W. T. S. Huck, Uniaxial alignment of liquid-crystalline conjugated polymers by nanoconfinement, *Nano Letters* **7[4]** (2007) 987-992.

[29] D. Cui, H. Li, H. Park, X. Cheng, Improving organic thin-film transistor performance by nanoimprint-induced chain ordering, *Journal of Vacuum Science & Technology B* **26[6]** (2008) 2404-2409.

[30] M. Zhou, M. Aryal, K. Mielczarek, A. Zakhidov, W. Hu, Hole mobility enhancement by chain alignment in nanoimprinted poly(3-hexylthiophene) nanogratings for organic electronics, *Journal of Vacuum Science & Technology B* **28[6]** (2010) C6M63-C6M67.

[31] T. T. Ngo, D. N. Nguyen, V. T. Nguyen, Glass transition of PCBM, P3HT and their blends in quenched state, Advances in Natural Sciences: *Nanoscience and Nanotechnology* **3** (2012) 045001.

[32] H. Hlaing, X. Lu, T. Hofmann, K. G. Yager. C. T. Black, B. M. Ocko, Nanoimprint-induced molecular orientation in semiconducting polymer nanostructures, *ACS Nano* **5[9]** (2011) 7532-7538.

[33] M. Aryal, K. Trivedi, W. (Walter) Hu, Nano-confinement induced chain alignment in ordered P3HT nanostructures defined by nanoimprint lithography, *ACS Nano* **3[10]** (2009) 3085-3090.

[34] D. Chen, A. Nakahara, D. Wei, D. Nordlund, T. P. Russell, P3HT/PCBM bulk heterojunction organic photovoltaics: Correlating efficiency and morphology, *Nano Letters* **11** (2011) 561-567.

[35] A. Baba, N. Aoki, K. Shinbo, K. Kato, F. Kaneko, Grating-coupled surface plasmon enhanced short-circuit current in organic thin-film photovoltaic cells, *ACS Applied Materials & Interfaces* **3[6]** (2011) 2080-2084.

CHAPTER III

DUAL PLASMONIC ENHANCED ORGANIC POLYMER SOLAR CELLS BY INCORPORATING SILVER NANODISKS INTO HOLE-TRANSPORT LAYER AND GRATING STRUCTURE ON TOP ELECTRODE

3.1 ABSTRACT

In this work, we designed the nanoengineering of metallic nanostructures to enhance light harvesting of organic polymer thin film solar cells (OPSCs) by dual surface plasmon resonance (SPR) phenomena originated from grating-coupled configuration with Blu-ray disc recordable (BD-R) grating of current collector and addition of silver nanodisks (Ag NDs) series. Different types and sizes of metallic nanoparticles (NPs), gold (Au) NPs, Ag nanospheres (NSs), and Ag NPs, were employed for our study and blended separately into a PEDOT:PSS hole transport layer (HTL). The best devices of grating-imprinted structure Al/P3HT:PCBM/Ag NDs:PEDOT:PSS/ITO were fabricated. The results from *J-V* curves indicated that the power conversion efficiency (PCE) of grating substrate Al/P3HT:PCBM/PEDOT:PSS/ITO was 3.10 % which was better than that of flat substrate for 1.55 times while devices with flat Al and addition of Au NPs, Ag NSs, or Ag NDs in a HTL performed with the PCEs in a range of 3.15-3.37. We further developed the OPSCs with Al grating substrate by incorporating Ag NDs series into a PEDOT:PSS layer. The PCEs of the devices were increased around 11-21% as compared to that of a pristine device. This indicated that the light absorption enhancement at the active layer is attributed to GCSPR and LSPR excitation with strong near-field distributions penetrated into absorption polymer, which could lead to higher efficiencies, thus resulting in better current generation.

3.2 INTRODUCTION

Organic polymer solar cells (OPSCs) with a bicontinuous interpenetrating network between the polymer donor and fullerene acceptor exhibit potential advantages as lightweight, flexible, large area devices and the low cost roll-to-roll fabrication [1-5]. Despite the fact that the efficiencies of the OPSCs have increased to 10.6 % [6], their power conversion efficiencies (PCEs) are still lower than those of their inorganic counterparts that approach efficiencies of

more than 20 % [7]. Typically, the PCEs of OPSCs are limited because of the weak absorbance of the thin photoactive layer in the solar spectrum range. To solve this problem, the thickness of the active layer should be increased for better absorption of the incoming photons. However, a thick active layer increases the series resistance of the device, causing the limited charge carrier mobility of the polymers. Therefore, many techniques have been developed for, in turn, governing efficient optical absorption in films rather than the improvement of the optical absorption depth. Thus, surface structures of each OPSC component such as periodic patterns or rough surfaces can increase the effective optical path of incident light inside absorbing materials by light trapping or scattering.

Recently, several light-trapping methods for OPSCs were investigated following the developments of wave-optics and nanotechnology. By scattering light into active layers with nanoparticles (NPs) [8-9] or textured substrates [10-11], light absorption has been enhanced generally [13]. Plasmonic effect for enhanced optical absorption were obtained through many ways such as excitation of localized surface plasmon resonance (LSPR) at metal NPs, propagation of surface plasmon polariton (SPP) modes and scattering of plasmonic enhancement [14-16].

In the majority of the imprinting processes, nanoimprinting lithography technique (NIL) is one of the alternative methods because of its simplicity for transferring pattern from a master mold to surface of the substrate [17]. Moreover, NIL process has been realized as a faster imprinting process, obtaining large nanopatterned areas [18]. Usually, polydimethylsiloxane (PDMS) was used as patterning master mold in this technique [19]. The PDMS mold works with fully complete conformal contact in patterning the substrate surface, even for the substrates with uneven surfaces. Compared to conventional photolithography, this soft lithography with the elastomeric PDMS mold has several advantages, especially patterning

the sensitive materials such as polymers, low cost, and no optical diffraction limit. It allows control of the chemistry, patterning of large areas, and scalable production for the patterned surfaces. Therefore, in the field of solar cells, in order to improve their performances, this NIL process has been recently employed for creating the irregular nanoscale features surface by nanoporous anodic aluminum oxide (AAO) membrane filters [20], the formation of ordered nano/microstructures by large-scale nanoporous Si mold and AAO templates [21-22], and formation of grating structure by Blu-ray movie discs (BD) and blu-ray disc-recordable (BD-R) [23-24]. The latter involves plasmonic effect at patterned metallic electrodes. Recently, a few studies have been demonstrated the nanoimprinting or grating-coupled process to fabricate periodic 1D grating-structure at cathode metallic electrode using BD-R in order to enhance the electric fields in photoelectric conversion systems [24]. The grating-coupled technique is a prism-less, convenient, propagating SPR excitation method [25-27]. In the absence of SP excitation, light scattering and light trapping can occur on the grating-structure surface, improving the obtained photocurrent [28]. Hence, dramatic improvement in photovoltaic cells is expected if, in addition to light scattering, the SP field can be enhanced on the grating substrate [29].

Interestingly, by utilizing the LSPR effect of metallic nanoparticles (NPs) such as Au nanoparticles (Au NPs) and Ag nanoparticles (Ag NPs), they can be introduced into each part of OPSC devices for highly improved light harvesting [30-33]. Although some reports showed excellent %PCEs by incorporating different kinds of metallic NPs into OPSCs [34-37], their influences on charge separation and transport inside high efficiency BHJ OPSCs still needs to be studied in depth. Many research groups reported the presence of Ag NPs in the PEDOT:PSS HTL of OPSCs exhibits enhanced light harvesting performances due to their superior scattering efficiency compared to those of any other metallic NPs [38]. Moreover, incorporating of Ag NDs in OPSCs has not been report. Silver nanodisks (Ag NDs), a type of Ag nanoprisms, have

attracted considerable attention due to their extreme degrees of anisotropy, morphologically dependent plasmonic properties, and wide range of light absorption and light scattering from visible to near infrared regions [39-41]. Use of Ag NDs in OPSCs has not been reported nowadays. It is expected that addition of Ag NDs, light absorption, light scattering and light trapping in OPSCs would be improved. Consequently, Ag NDs were chosen in this research work.

From discussion above, both plasmonic effects, namely NP plasmons and SPP, which perform synergistically, are of interest in developing new generation of plasmonic photovoltaic cells. Improving light trapping as well as managing light harvesting in OPSCs would be obtained with the plasmonic effects such as LSPRs from two different metallic NPs (Ag NPs + Au NPs) or LSPRs from two different shapes (Au nanorods + Au nanospheres) and LSPR-GCSPR effect from (Au NPs + Ag NPs + 1D grating-structure Al electrode). Excitation of free electrons in metal NPs or at metal/dielectric interfaces results in the storage of energy in the LSPR at the NPs or in the SPPs at the metal/dielectric interfaces, which could be converted into absorption events in the semiconductor via either a near field effect or a far-field coupling. In this study, we designed and fabricated OPSCs based on the imprinted 1D grating structures on the active layer of organic thin film as support of Al electrode and incorporating Ag NDs series into HTL in BHJ solar cell for improving the light trapping via the dual plasmonic effects of the grating-structure al and the metal NPs. Cooperative dual plasmonic effect exhibits the advantages such as broader light absorption enhancement, enhanced exciton generation rate and dissociation efficiency and increased charge carrier density and lifetime. Moreover, finite-difference time-domain (FDTD) simulations were performed to investigate the electric field distribution around the Ag NDs series surfaces and metallic grating, confirming dual plasmonic effect.

3.3 EXPERIMENTAL DETAILS

3.3.1 Synthesis of Ag nanodisks

The synthesized procedures of Ag NSs and Ag NDs were according to the literature [41-42]. Firstly, synthesis of Ag NSs by chemical reduction method was carried out using $NaBH_4$ (Merck) as a reducing agent. 0.63 g $AgNO_3$ (Merck) was dissolved in 500 mL starch solution and then $AgNO_3$ solution was injected into the 500 mL of $NaBH_4$, which was dissolved in starch solution, with control injection rate at 2.0 mL s^{-1} under a vigorous stir. The reaction mixture was stirred at room temperature for 30 min and boiled for 2 hr. Then, the solution was left to room temperature and aged for 12 hr to ensure an elimination of residual $NaBH_4$. Upon completion, Ag NSs solution was collected and adjusted to 1000 mL with DI water. Finally, the Ag NSs were obtained and stored at 4 °C before use (within 24 hr). The diameters of the Ag NSs were in a range of 6-7 nm. The Ag NDs were synthesized via a chemical shape transformation of Ag NSs. 2.272 mL of 30% w/w H_2O_2 (Merck) solution was injected into a 200 mL of Ag NSs colloid by syringe pump using the rate at 13.45 mL min^{-1} under a vigorous stir. Because the molar ratio of H_2O_2:Ag NSs is the key parameter for controlling the LSPR wavelengths of Ag NDs, in this study it was varied from 0 to 15. After the addition of H_2O_2 solution, the colloid solution was further stirred for another 10 min to ensure a complete reaction and the average diameters of Ag NDs were ranging of 30-70 nm.

3.3.2 Preparation of grating mold for imprinting Al electrode of organic polymer solar cells

The grating structure was duplicated from BD-R master template. First step, peeling polycarbonate layer, peeling aluminum layer and etching the grating substrate were obtained in conc. HNO_3 for 20 min. Then, the grating substrate was cleaned subsequently using detergent, distilled water, and deionized water by ultrasonication for 20 min for each step after

that drying the substrate by flow N_2 gas and cutting grating substrate to the size of 2.5 x 2.5 cm^2 were performed. Preparing the PDMS by mixing silicone elastomer base and silicone elastomer curing agent in a ratio of 10:1 (13 g) was carried out in the plastic glass under stirring. The PDMS was poured onto the master template and the air bubble in PDMS was removed at 70^oC in a vacuum oven for 3 h. After cooling to room temperature, the master template was detached from the PDMS duplicate.

3.3.3 Preparation of solar cell devices

Indium-doped tin oxide (ITO) glass substrates (FINE brand, Furuuchi Co. Ltd., 10 Ω/cm^2) were cleaned by using detergent, distilled water and deionized water by 20 min ultrasonication for each step and then dried in a nitrogen gas flow. After drying, the substrates were exposed to ultraviolet ozone plasma for 20 min. The hole transporting material (HTM) PEDOT:PSS solution (Clevios, Heraeus Co.) was blended with 20 %v/v of metallic NPs (Ag NSs). The mixture solution was spin-coated onto the ITO substrate at 1000 rpm for 90 s and the resultant substrate was dried at 120^oC in a vacuum oven for 10 min. Poly(3-hexylthiophene) (P3HT) (Sigma-Aldrich) and phenyl C61-bytaric acid methyl ester ($PC_{61}BM$) (Sigma-Aldrich) were mixed at a weight ratio of 1:0.8 in 1.0 ml 1,2-dichlorobenzene (Kanto chemical Co.) for 24 h. The photoactive layer was spin-coated at 1000 rpm for 15 s and 1500 rpm for 45 s, respectively, and imprinted with the grating pattern PDMS mold by thermal imprinting process at 100^oC in a vacuum oven for 60 min. The devices were deposited thin aluminum (150 nm) by vacuum evaporation technique. Finally, the device was annealed at 150^oC for 45 min in a vacuum oven. The active areas of these devices are of 1.0 cm^2. The devices based on Au NPs (Sigma-Aldrich) and Ag NDs with different diameters including 30, 40, 50, and 70 nm added into PEDOT:PSS layer were prepared using the similar process. Figure 3.1 shows fabrication of OPSC devices. In addition, the reference cells were prepared with the same configuration with no NPs and Al grating.

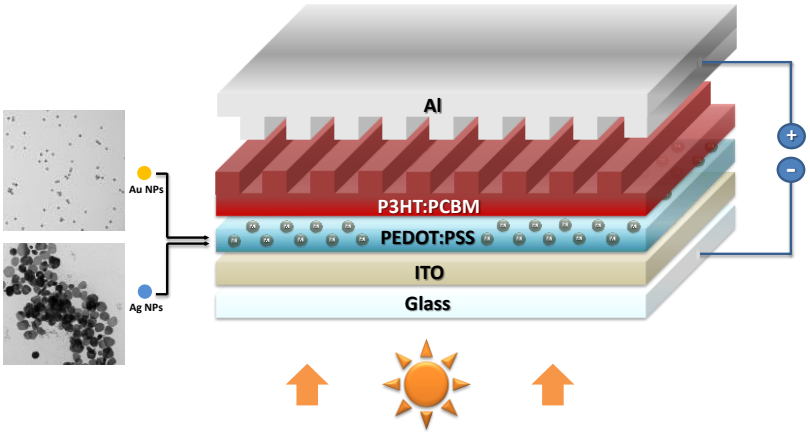

Figure 3.1 Schematic of organic polymer solar cell devices.

3.3.4 Characterization

The optical properties of materials and devices were investigated using a UV-visible spectrophotometer (V-650, Jasco). Morphology of Ag NDs series was studied using transmission electron microscopy (TEM, JEOL Ltd., USA). An atomic force microscope (AFM, SPM-9600, Shimadzu) was used to analyze the surface morphology of the prepared films. Under an ambient environment, current density–voltage (*J*-*V*) curves and impedance spectra of all the fabricated OPSCs under irradiating were recorded employing a solar simulator (HAL-C100, 100 W compact xenon light source, Asahi Spectra) equipped with a precision source-meter unit (B2901A, Agilent) and a potentiostat (PARSTAT 4000, Princeton Applied Research). The solar cell was operated under illumination with a light intensity of 75 mW cm^{-2}. A quantum efficiency measurement kit (Newport-serial number 425) embedded in the solar simulator was used to obtain external quantum efficiency (EQE) values. Merlin monochromator with a 300W Xenon arc lamp was used as a light source to provide throughput to the cells in the experiment.

3.4 RESULTS AND DISCUSSION

To study the effect of incorporating plasmonic nanostructures into the solar cell devices, the active layer was imprinted with grating structure and the HTL was incorporated with metallic NPs. The optimizations of active layer film thickness and NPs content and type of NPs were also studied. In our experiment, we designed the cells as follows:

1. Control device (Figure 3.2(a)): Al/P3HT:PCBM/PEDOT:PSS/ITO
2. Device with grating structure (Figure 3.2(b)): grating-patterned Al/P3HT:PCBM/PEDOT:PSS/ITO
3. Device with metallic NPs (Figure 3.2(c)): Al/P3HT:PCBM/(Au NPs or Ag NPs or Ag NDs series:PEDOT:PSS/ITO
4. Device with grating structure and metallic NPs (Figure 3.2(d)): grating-patterned Al/P3HT:PCBM/(Au NPs or Ag NPs or Ag NDs series:PEDOT:PSS/ITO

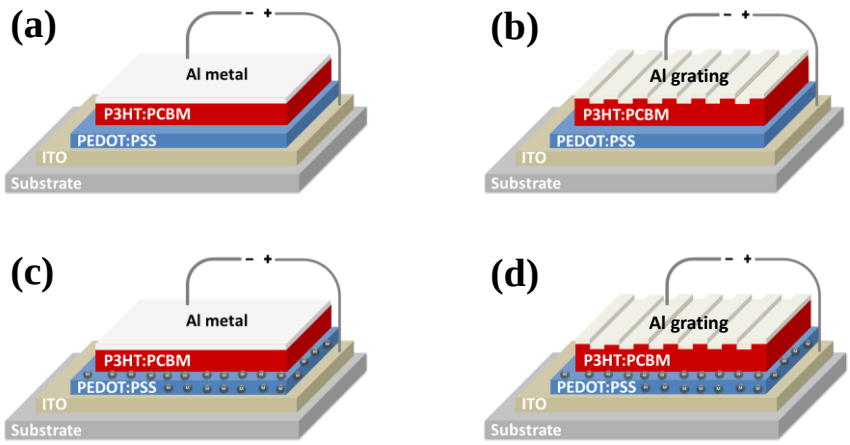

Figure 3.2. Fabrication of our experiment (a) control device (b) device with grating structure (c) device with metallic NPs (d) device with grating structure and metallic NPs.

To study the particles shapes and sizes of the metallic NPs, TEM images of the mono-dispersed Au NPs, Ag NSs and Ag NDs series are shown in Figure 3.3. It can be seen that the

Au NPs are spherical in shape and highly dispersed with an average diameter of 5 nm. In the case of Ag NDs series, after injection of H_2O_2 into the Ag NSs solution, the color of the solution instantaneously changed from yellow to red, pink, violet, or blue depending on the molar ratio between H_2O_2 and Ag NSs. The result from TEM shows the well-dispersed Ag NDs series in deionized water and their average diameters ranging from 30 - 70 nm, denoted as Ag NDs-30, Ag NDs-40, Ag NDs-50 and Ag NDs-70, respectively. Therefore, it is plausible that Ag NDs series can be imbedded within PEDOT:PSS layer (100 nm) and it is expected that LSPR of Ag NDs would be induced near the active layer of our devices.

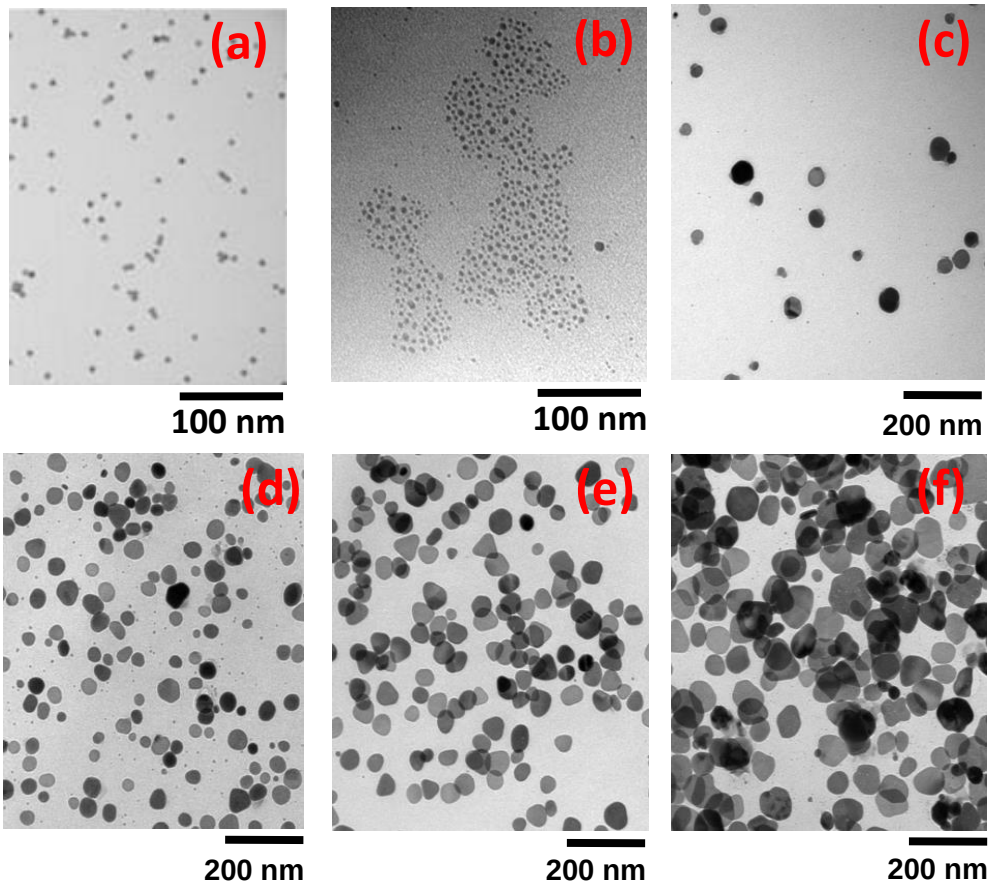

Figure 3.3 TEM images of Au NPs, Ag NSs and Ag NDs with different maximum absorption peaks at a) 510 nm, b) 535 nm, c) 570 nm, and d) 660 nm.

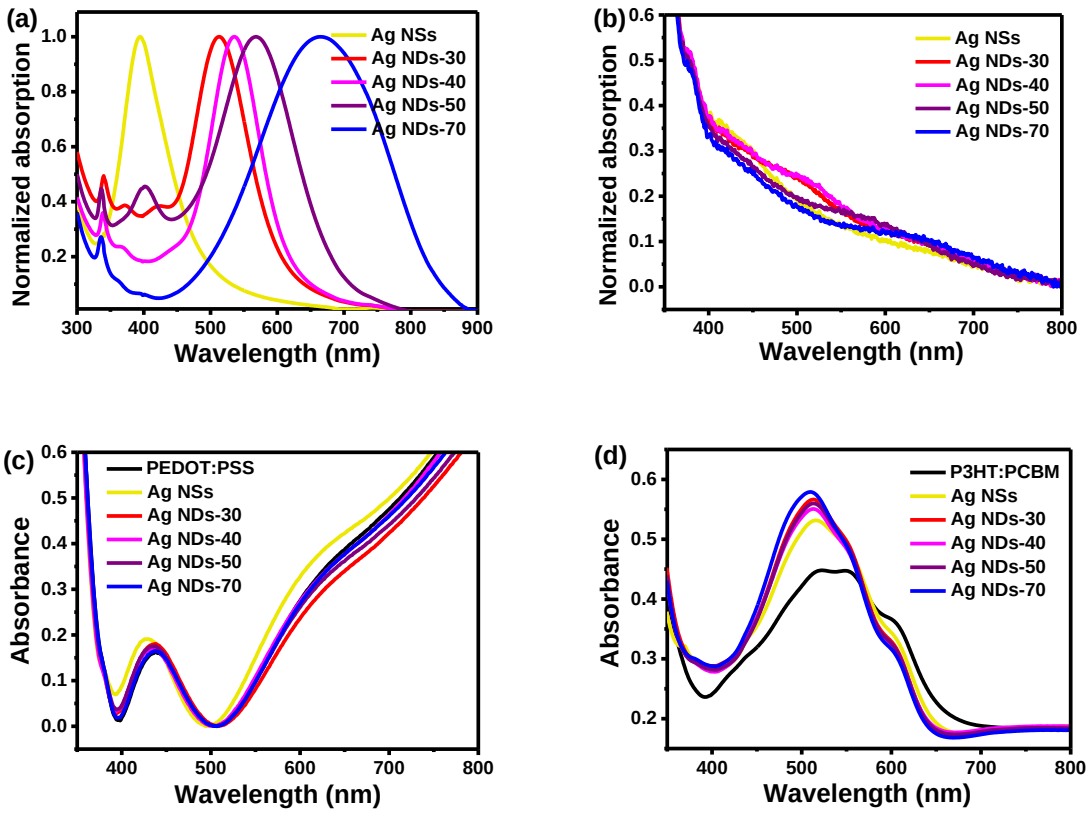

Figure 3.4 UV-visible absorption spectra of (a) Ag NPs in solutions, (b) ITO/Ag NPs film, (c) ITO/PEDOT:PSS/Ag NPs film, and (d) ITO/PEDOT:PSS/Ag NPs/P3HT:PCBM film.

The optical absorbances of Au NPs, Ag NSs, or Ag NDs series solutions and of PEDOT:PSS films incorporated with Au NPs, Ag NSs, or Ag NDs series were measured by a UV-visible spectrometer. It can be seen that the plasmonic resonance peak of Au NPs in the solution exhibits at 520 nm (Figure A2.1). Figure 3.4(a) exhibits the plasmonic resonance peaks of Ag NSs, Ag NDs-30, Ag NDs-40, Ag NDs-50 and Ag NDs-70 in the solution phase at 410, 510, 535, 570 and 660 nm, respectively. It was found that the color and spectral changes directly associated with the morphological transformation of the Ag NPs. Moreover, the absorption peaks of Ag NSs and Ag NDs series films were also studied as shown in Figure 3.4(b). It was found that the plasmonic resonance peaks of Ag NSs film, Ag NDs-30 film, Ag NDs-40 film, Ag NDs-50 film and Ag NDs-70 film exhibit a small single peak in the visible range at 410, 510, 535, 570 and 660 nm, respectively. This indicates that size and shape of Ag

NDs have no significant changes in dried state (film). In addition, the absorption spectra of ITO/PEDOT:PSS/Ag NSs or Ag NDs series films were also measured as shown in Figure 3.4(c). Moreover, the absorption profiles of PEDOT:PSS film on ITO with and without addition of the NPs are not significantly different over a region of 500 - 800 nm. In the other hand, the absorption intensities of ITO/PEDOT:PSS/P3HT:PCBM films after addition of Ag NSs or Ag NDs series are significantly chanced as shown in Figure 3.4(d). It was found that the absorption of the active layer has been obviously enhanced with increasing diameter of Ag NDs due to their scattering effect [42].

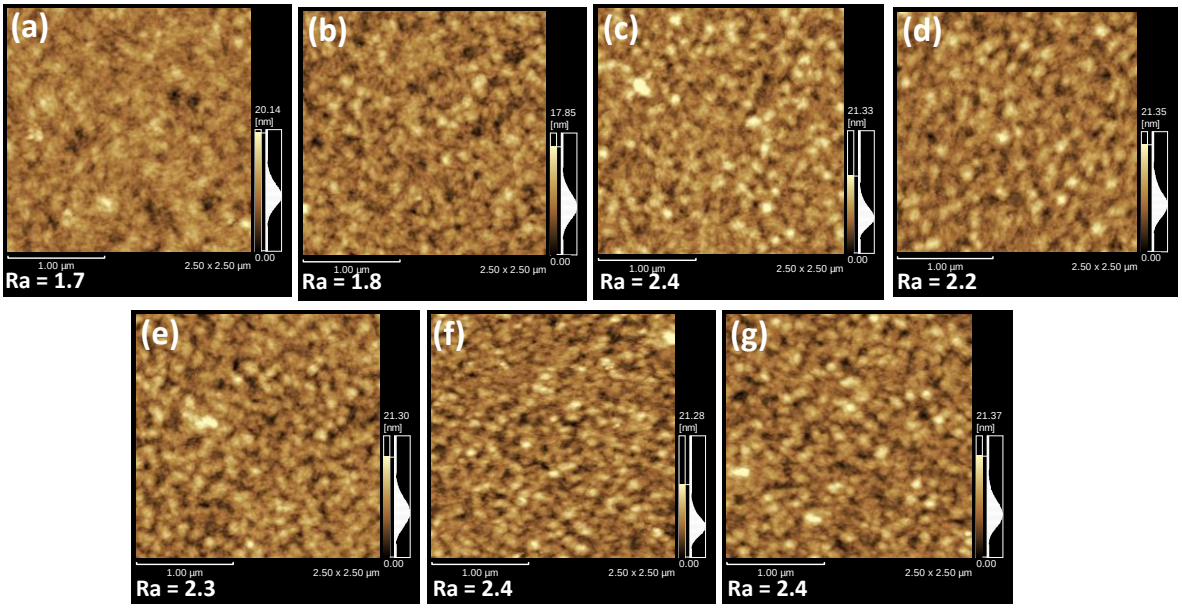

Figure 3.5 AFM images of bare PEDOT:PSS film (a), PEDOT:PSS film incorporated with Au NPs (b), Ag NSs (c), Ag NDs-30 (d), Ag NDs-40 (e), Ag NDs-50 (f), and Ag NDs-70 (g), respectively.

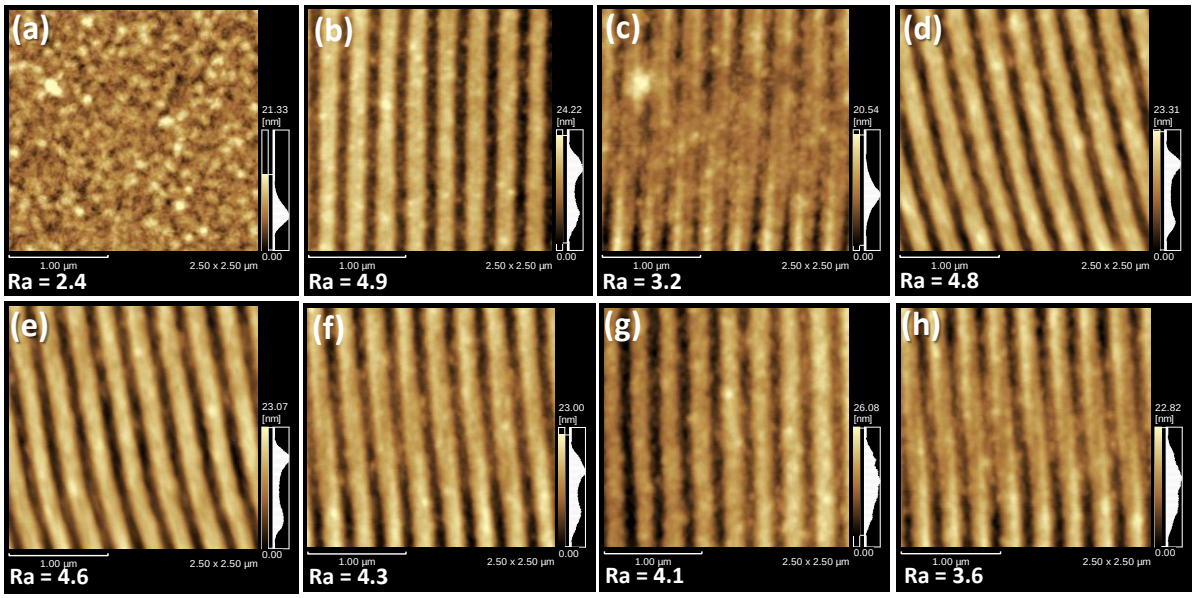

Figure 3.6 AFM images of bare active layer (a), grating-imprinted active layer (b), and grating-imprinted active layers on PEDOT:PSS films blended with Ag NPs (c), Ag NSs (d), Ag NDs-30 (e), Ag NDs-40 (f), Ag NDs-50 (g), and Ag NDs-70 (h).

The AFM images of PEDOT:PSS HTLs with and without metallic NPs are shown in Figure 3.5. The root-mean-squared (RMS) roughness (R_a) of PEDOT:PSS layer on ITO glass was measured to be 1.7 nm (Figure 3.5(a)) while those of PEDOT:PSS blended with Au NPs, Ag NSs, Ag NDs-30, Ag NDs-40, Ag NDs-50, or Ag NDs-70 exhibited the R_a values of 1.8, 2.4, 2.2, 2.3, 2.4, or 2.4 nm, respectively (Figure 3.5(b)-(g)). It is indicated that all the metallic NPs increase the R_a of PEDOT:PSS HTL. Furthermore, the morphology of the active layer after imprinting with 1D grating was observed as shown in Figure 3.6. The R_a of active layer on PEDOT:PSS-coated ITO glass was measured to be 2.4 nm (Figure 3.6(a)) while active layer after imprinting with the 1D grating was measured to be 4.9 nm (Figure 3.6(b)). Moreover, the R_a values of the photoactive layer imprinted with the 1D grating, on PEDOT:PSS HTLs containing Au NPs, Ag NSs, Ag NDs-30, Ag NDs-40, Ag NDs-50, or Ag NDs-70, were 3.2, 4.8, 4.6, 4.3, 4.1, or 3.6 nm, respectively Figure 3.6(c)-(h). It is noted that the active layer imprinted with 1D grating has a R_a value higher than those of the grating-imprinted active

layers sitting on HTL blended with a variety of metallic NPs. As a result, the addition of metallic NPs into HTL lead to decrease the R_a of the device photoactive layers. Moreover, an increase in nanoparticle size of Ag NDs in PEDOT:PSS layer decreased the R_a of the layers.

To obtain the best performances of the devices with 1D Al grating and metallic NPs-containing HTL, the active layer thickness is necessary to be optimized due to its limited absorption ability of light and exciton generation [43]. In this study, the thickness of active layer in the device was varied by the spin-coating rate for 90 s. Spin-coating rates, i.e. 1000, 1500, 2000, and 2500 rpm gave the film thickness of *ca*. 60 nm, 80 nm, 100 nm and 120 nm, respectively. Consequently, we studied the effect of active layer thickness on device performances for the four device fashions: reference device, device with Al grating, device with HTL containing metallic NPs such as Au NPs or Ag NDs having the same plasmonic resonance peak, and device based on imprinted Al electrode and HTL incorporated with Au NPs or Ag NDs. Figure 3.7 shows plot of %PCE against thickness of active layer for three device systems and Table 3.1 shows the PCE values of their fabricated devices. It is clearly observed that the control device exhibits the best PCE of 2.98% at the thickness layer of 100 nm while the device with grating-imprinted Al exhibit the best PCE of 3.16% at the thickness layer of 120 nm. Moreover, the devices incorporated with Au NPs and Ag NDs possessing the plasmonic resonance peak around 520 nm exhibit the best PCEs of 3.25% and 3.39%, respectively, at the thickness layer of 80 nm. Furthermore, the devices imprinted with 1D grating and incorporated with Au NPs or Ag NDs exhibit the best PCEs of 3.36% and 3.42%, respectively, at the thickness layer of 100 nm. The active layer with 100 nm in thickness was, therefore, chosen for next study.

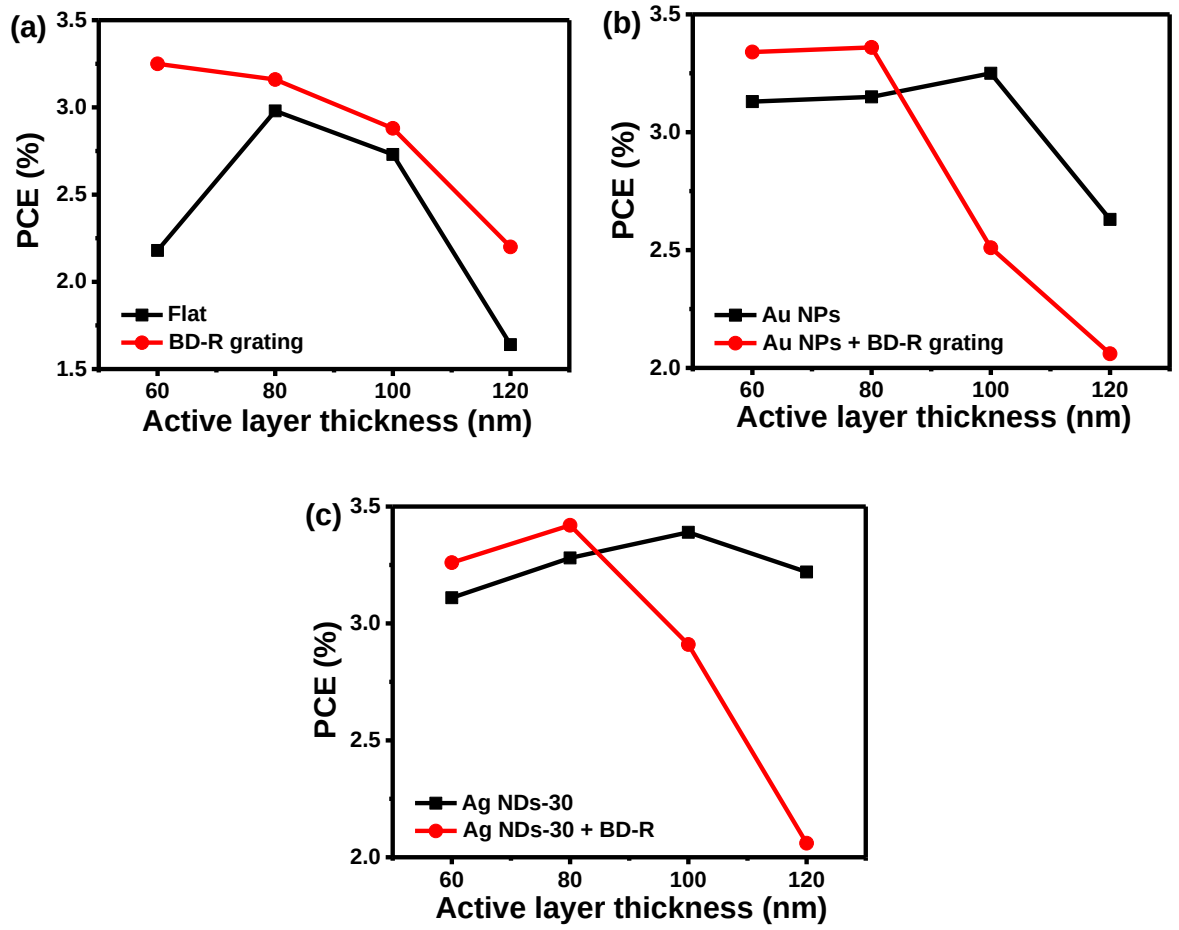

Figure 3.7 Effect of active layer thickness on device performance (PCE (%)) of OPSCs: (a) without addition of metal NPs, (b) with Au NPs in HTL and (c) with Ag NDs-30 in HTL.

Table 3.1 PCE of OPSCs with different thicknesses of photoactive layer.

Spin-coating rate (rpm)	Thickness (nm)	%PCE					
		Control device	Al grating	Ag ND-30		Au NPs	
				w/o Al grating	w Al grating	w/o Al grating	w Al grating
1000	120	2.18	3.25	3.11	3.26	3.13	3.34
1500	100	2.98	3.16	3.28	3.42	3.15	3.36
2000	80	2.73	2.88	3.39	2.91	3.25	2.51
2500	60	1.64	2.20	3.22	2.06	2.63	2.06

Note: w/o = without, w = with

To investigate the effect of the different kinds of metallic NPs in OPSC, we demonstrated the two solar cell systems based on PEDOT:PSS films containing Au NPs or Ag NDs-30 having the same resonance plasmonic peak (≈ 520 nm) and we also examined their dual plasmonic effect including the metallic NPs in the HTL and Al cathode with grating structure. The *J-V* curves for control device, device with Al grating cathode, device with Au NPs-incorporated HTL, device with Ag NDs-30-incorporated HTL, device with Au NPs-blended HTL and imprinted Al grating, and device with Ag NSs-mixed HTL and grating structure Al are shown in Figure 3.8. The photovoltaic performances of such solar cell devices are listed in Table 3.2. It was found that incorporating Au NPs in HTL increased the short-circuit current densities (J_{sc}) of the device from 6.42 to 6.87 mA/cm^2 while no significant changes in open-circuit voltage (V_{oc}) and FF were observed. As the result, PCE was enhanced from 2.98% to 3.15%. In the same way, incorporating Au NDs-30 into HTL exhibited the improvement of the device performances. The enhanced J_{sc} value of 7.10 mA/cm^2, enhanced V_{oc} value of 0.63 V, improved FF value of 0.55, and PCE of 3.27% were observed in this system. This indicates that presence of either Au NPs or Ag NDs in PEDOT:PSS HTL would enhance the solar cell performances by the LSPR effect [30-31]. To investigate the grating structure effect on the light harvesting, patterning Al cathode of OPSCs was demonstrated. Grating structure on the active layer of OPSC finished by Al deposition also leads to an improvement of the OPSC performance (see Figure 3.8). It can be seen that with grating structure, the J_{sc} value increased around 8% and the PCE increased to 3.16%. This would involve light scattering by grating structure, which results in an increment of the light traveling path inside the active layer, thereby increasing the light absorption by the active layer. Furthermore, the strong electric field originated from GCSPR of the metallic grating can also enhance the generation of the photocurrent, which results in an increase of J_{sc} and PCE [23]. Moreover, we studied the dual plasmonic effect including the metallic NPs in HTL and grating

architecture on Al cathode. It was found that the solar cell based on Au NPs-incorporated HTL and imprinted Al cathode exhibit the performance better than that of the device with Al grating and no addition of Au NPs. The dual plasmonic system based on Au NPs provided the device with increased J_{sc} value of 7.44 mA/cm^2, no significant change in V_{oc} and FF values, and resultant enhanced %PCE of 3.36. Similarly, the device containing Ag NSs-30 in HTL and grating-imprinted Al electrode showed the higher performance as compared to the imprinted device with no addition of Ag NSs-30. Enhanced performances, namely J_{sc} of 7.32 mA/cm^2, V_{oc} of 0.63 V, FF of 0.56, and PCE of 3.42% were found for this device. Therefore, it can be seen that the devices imprinted with grating and incorporated with the metallic NPs would perform by light scattering effect and LSPR of the metallic NPs and GCSPR of grating structure Al cathode [24, 30-31]. Moreover, it can be clearly observed that the imprinted device incorporated with Ag NDs-30 into HTL exhibited the best performance, which would be resulted from the higher light scattering of the Ag NDs [44]. In this work, we are interested in light harvesting management using Ag NDs series together with metallic grating to achieve the broadband plasmonic absorption as well as the highest device performances.

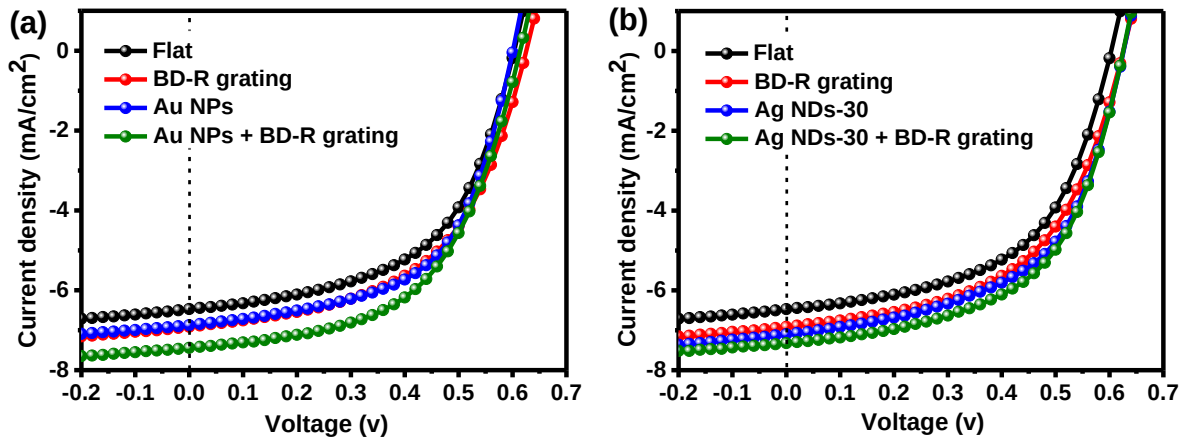

Figure 3.8 *J–V* curves of the device systems: (a) Au NPs and (b) Ag NDs-30 incorporated into PEDOT:PSS layer.

Table 3.2 Photovoltaic performances of all solar cell devices from Figure 3.8.

Devices	J_{SC} (mA/cm^2)	V_{OC} (V)	FF	PCE (%)	Improvement (%)
Control device	6.42	0.60	0.58	2.98	
BD-R grating	6.99	0.61	0.55	3.16	6.04
Au NPs	6.87	0.60	0.57	3.15	5.70
Au NPs + BD-R grating	7.44	0.61	0.55	3.36	12.75
Ag NDs-30	7.01	0.63	0.55	3.27	9.73
Ag NDs-30 + BD-R grating	7.32	0.63	0.56	3.42	14.76

To study the effect of Ag NDs series and its dual plasmonic configuration on light harvesting ability, the photocurrents of OPSCs were measured under AM 1.5G illumination at 75 mW/cm^2. Corresponding *J-V* curves of devices with and without addition of Ag NDs series, grating structure Al cathode and the dual plasmonic system in comparison with that of control device are shown in Figures 3.9(a) and (b). Table 3.3 shows the summary of performances and properties of such solar cells. There are a few reports about employing Ag NPs together with patterned Al for construction of OPSCs. In present research, we first studied the improvement of light harvesting by incorporating Ag NSs and Ag NDs series including Ag NDs-30, Ag NDs-40, Ag NDs-50 and Ag NDs-70 into HTL (Figure 3.9(a)), as well as additionally by imprinting Al with grating (Figure 3.9(b)). It was found that after incorporating Ag NDs series into PEDOT:PSS layer, J_{sc} increased to 7-10 and V_{oc} increased to 5-6%, while FF remained nearly the same and the PCE slightly increased with increasing the diameter of Ag NPs. The PCE increased from 2.98% to 3.22%, 3.27%, 3.29%, 3.33% and 3.37% when devices were constructed using Ag NSs, Ag NDs-30, Ag NDs-40, Ag NDs-50 and Ag NDs-70 respectively, as compared with that of a control device fabricated in similar condition.

After incorporating Ag NSs and Ag NDs series into PEDOT:PSS layer, the improved performances of OPSCs might result from the following possible factors. First, the optical path length in the active layer can be increased because light was trapped through multiple and high-angle scattering from Ag NSs and Ag NDs series. According to the well-known Mie theory [45], the total Mie extinction is a sum of contributions from absorption and scattering components, and larger particles have a larger scattering cross section. Typically, the light scattering efficiency is lower than the light absorption efficiency for Ag NPs having particle sizes of less than 100 nm. The sizes of the Ag NSs and Ag NDs series used in this work are ranging from 6 to 70 nm. Moreover, the density of Ag NSs and Ag NDs series are relatively low, therefore, the light scattering is not the dominant mechanism for the improved device performance. Second, the LSPR of Ag NSs and Ag NDs series can produce large local electromagnetic fields near the nanoparticle surface and the resulting local field enhancement increases the light absorption of the organic materials, improving overall efficiency of device. With increasing particle size, the decay distance of local field may be increased, and furthermore, more Ag NSs and Ag NDs series covered with PEDOT:PSS will protrude into the active layer. Consequently, the near field will extend into the active layer at a large extent, and the possibility of interaction coupling between the near field and the incident light in the active layer will be increased, enhancing the photo-generation of excitons in the active layer. As a result, the PCEs of plasmonic solar cells rise with the increment of particle size of Ag NDs. In addition, the wavelength range of spectral response enhancement is consistent with the plasmon resonance peak of Ag NSs and Ag NDs series, indicating that the excitation of LSPR is responsible for the enhancement of PCE.

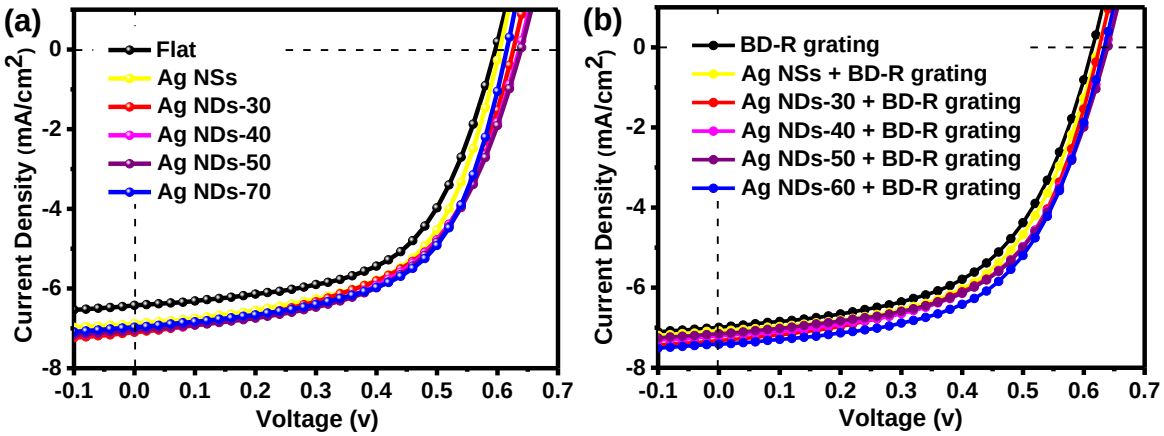

Figure 3.9 *J–V* curves of the devices incorporated with (a) different Ag NDs in PEDOT:PSS layer and (b) different Ag NDs in PEDOT:PSS layer and grating-imprinted Al electrode.

Interestingly, we observed that combining both plasmonic nanostructures, Ag NPs/Au NPs and metallic grating, into OPSCs showed preliminary excellent results, suggesting that the OPSCs harvest solar light with synergic effect of such plasmonics. To improve their performances, dual plasmonic effect originated from Ag NDs series and grating-coupled technique of Al cathode was achieved in our work. The dual plasmonic OPSCs were developed and designed as illustrated in Figure 3.9(d). The devices were imprinted with 1D grating structure followed by vacuum deposition of Al and incorporated with Ag NDs series in PEDOT:PSS layer. It was found that J_{sc} increased around 10-15% and V_{oc} increased around 3-7%, while FF seems to be decreased and the PCE enhanced from 2.98% to 3.32%, 3.42%, 3.42%, 3.43% and 3.59% for imprinted Al grating-based OPSCs with HTLs containing Ag NSs, Ag NDs-30, Ag NDs-40, Ag NDs-50 and Ag NDs-70, respectively. This indicated that the light absorption enhancement at the active layer is attributed to LSPR excitation with strong near-field distributions penetrated into absorption polymer and GCSPR from metallic grating, which lead to higher efficiencies due to the increased absorption, thus resulting in better current generation.

Table 3.3 Performances of different OPSCs from our work.

Devices	LSPR peak of Ag NDs (nm)	grating	J_{sc} (mA/cm^2)	V_{oc} (V)	FF	PCE (%)	Improvement (%)
Flat	-	-	6.42	0.60	0.58	2.98	-
Grating	-	-	6.99	0.61	0.55	3.16	6.04
Ag NPs	410	-	6.88	0.60	0.58	3.22	8.05
Ag NPs	410	+	7.08	0.62	0.56	3.32	11.41
Ag NDs-30	510	-	7.10	0.63	0.55	3.27	9.73
Ag NDs-30	510	+	7.32	0.63	0.56	3.42	14.76
Ag NDs-40	535	-	7.05	0.64	0.55	3.29	10.40
Ag NDs-40	535	+	7.21	0.64	0.56	3.42	14.76
Ag NDs-50	570	-	7.05	0.64	0.56	3.33	11.74
Ag NDs-50	570	+	7.15	0.64	0.56	3.43	15.10
Ag NDs-70	660	-	6.97	0.62	0.59	3.37	13.09
Ag NDs-70	660	+	7.41	0.63	0.57	3.59	20.47

To study the propagating SPR excitation on the Al grating, the reflectivity of the OPSCs on the irradiation of white light from the ITO glass side were measured from incident angle 20^o to 70^o as shown in Figure 3.10. The SPR reflectivity curves of the devices without a grating (flat Al) and with/without incorporating Ag NDs into HTL were observed in the wavelength region of 400-800 nm (Figures 3.10(a) and 3.10(c)). It was found that in wavelength region above 500 nm, no obvious dip peak at the resonant wavelength with *p*-polarized light was found as shown in Figures 3.10(a) and 3.10(c). On the other hand, Figures 3.10(b) and (d) exhibit the

SPR reflectivity curves of the devices with only Al grating and combination of Al grating and incorporating Ag NDs into HTL. Dip peak in each reflection spectrum due to the excitation of surface plasmon was observed in the range of 650-750 nm under *p*-polarized light irradiation. The red shift of the dip peak in the spectrum from 650 nm to 750 nm was upon increasing the incidence angle, thus confirming the SPR properties of the fabricated Al grating on top devices. This result indicates that the improvement in J_{sc} in the devices with 1D grating originated from the improvement in light absorption due to light scattering and GCSPR.

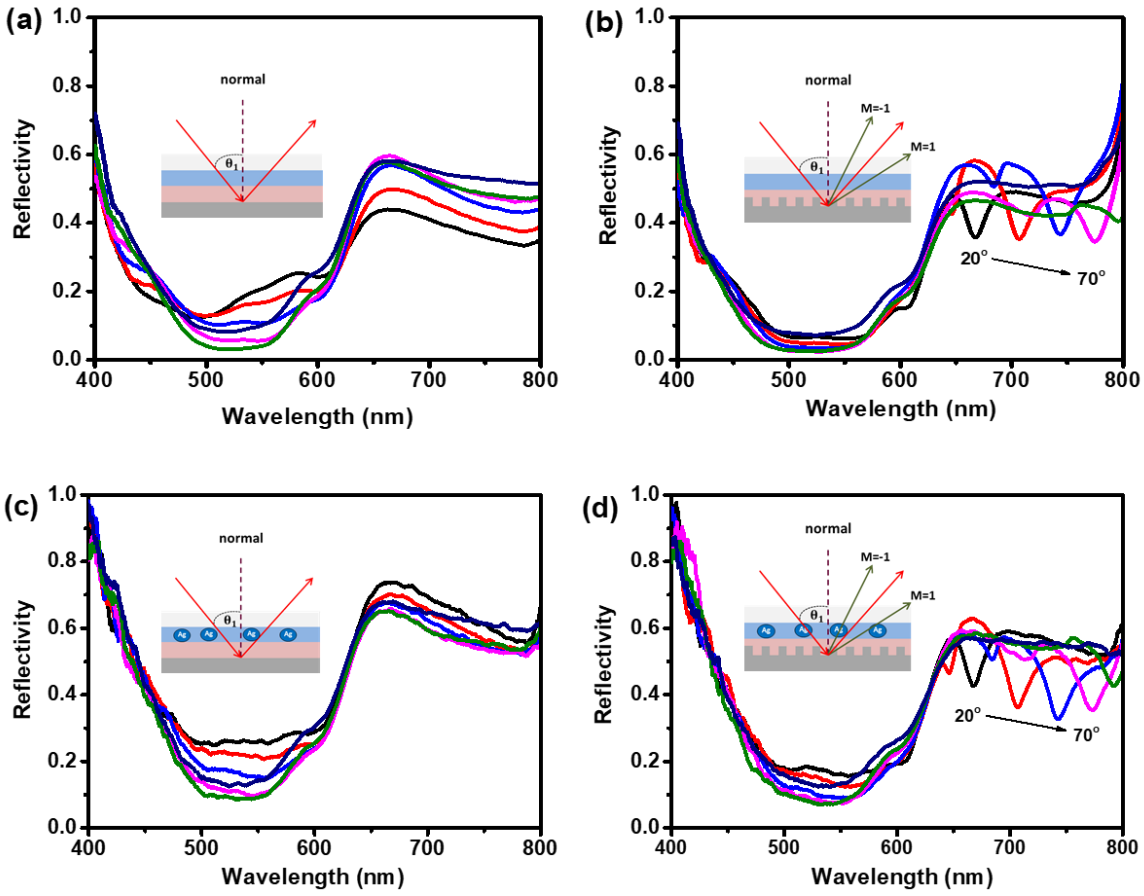

Figure 3.10 SPR reflectivity curves of the solar cells with *p*-polarization at various incident angles from 20° to 70° for (a) flat Al electrode, (b) grating Al electrode, (c) PEDOT:PSS incorporated with Ag NDs and (d) PEDOT:PSS incorporated with Ag NDs and grating Al electrode.

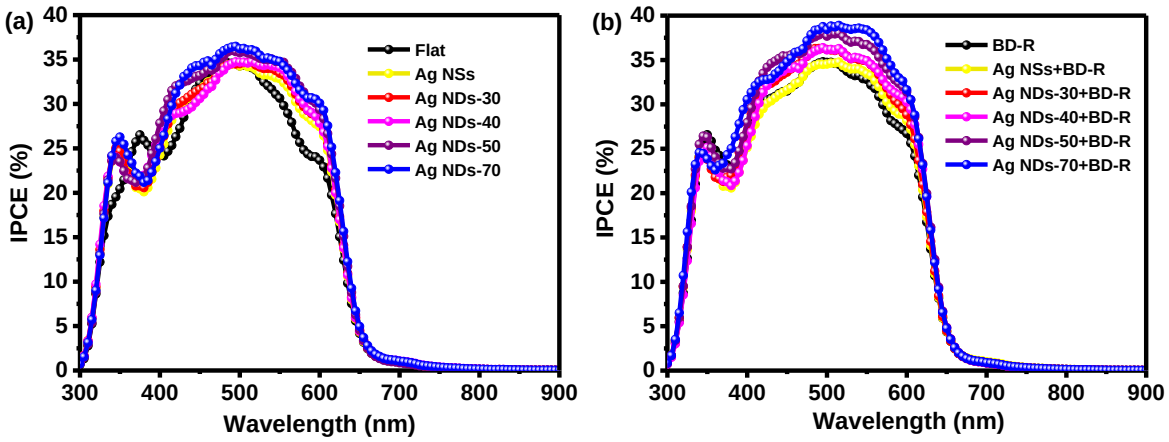

Figure 3.11 IPCE spectra of the devices incorporated (a) with different size of Ag NDs in PEDOT:PSS layer and (b) with different size of Ag NDs incorporated into PEDOT:PSS layer and grating-imprinted pattern on a top Al electrode.

To demonstrate the cooperative effect of Ag NSs or Ag NDs series and grating structure on improving devices performance by SPR in corresponding wavelength region, the incident photon-to-current efficiency (IPCE) spectra were observed as shown in Figures 3.11(a) and 3.11(b) for metallic NPs-added OPSCs without and with Al grating, respectively. The IPCEs of the both OPSC system incorporated with only Ag NDs series in HTL and the system with dual plasmonic configuration exhibited a higher IPCE than that of the control device. Moreover, with increasing particle size of Ag NDs, the IPCEs increased, which agree well with %PCE and current density results. To confirm and clarify the effect of Ag NDs and grating structure Al on light absorption in broadband wavelength range, the enhancement factor (E.F.) profiles, which the IPCEs of improved devices are divided by IPCEs of control devices, are shown in Figure 3.12. It is noted that for the device imprinted with grating structure the improved current can be generated from excitation of GCSPR in the range of 650-800 nm (Figure 3.12(a)), in which the maximum E.F. is related to incident angle, whilst for devices incorporated Ag NDs series, the current can be generated over a broad wavelength range from 400-650 nm, which is of the optical absorption and LSPR and light scattering effects of Ag

NDs (Figure 3.12(b)). In addition, light scattering would occur at Al grating, causing the improved photocurrent. Figure 3.12(c) shows the enhancement from only LSPR effect of Ag NDs (370-470 nm) and from light scattering effect (450-700 nm) from both Ag NDs and Al grating but no enhancement response of GCSPR of Al grating is not found since the measurement was undertaken at an incident angle of 0º. Therefore, the higher photocurrent of devices designed involving grating-coupled configuration and incorporating Ag NDs series into HTL is attributed to dual plasmonic effect (SP excitations), light absorption, light scattering and trapping.

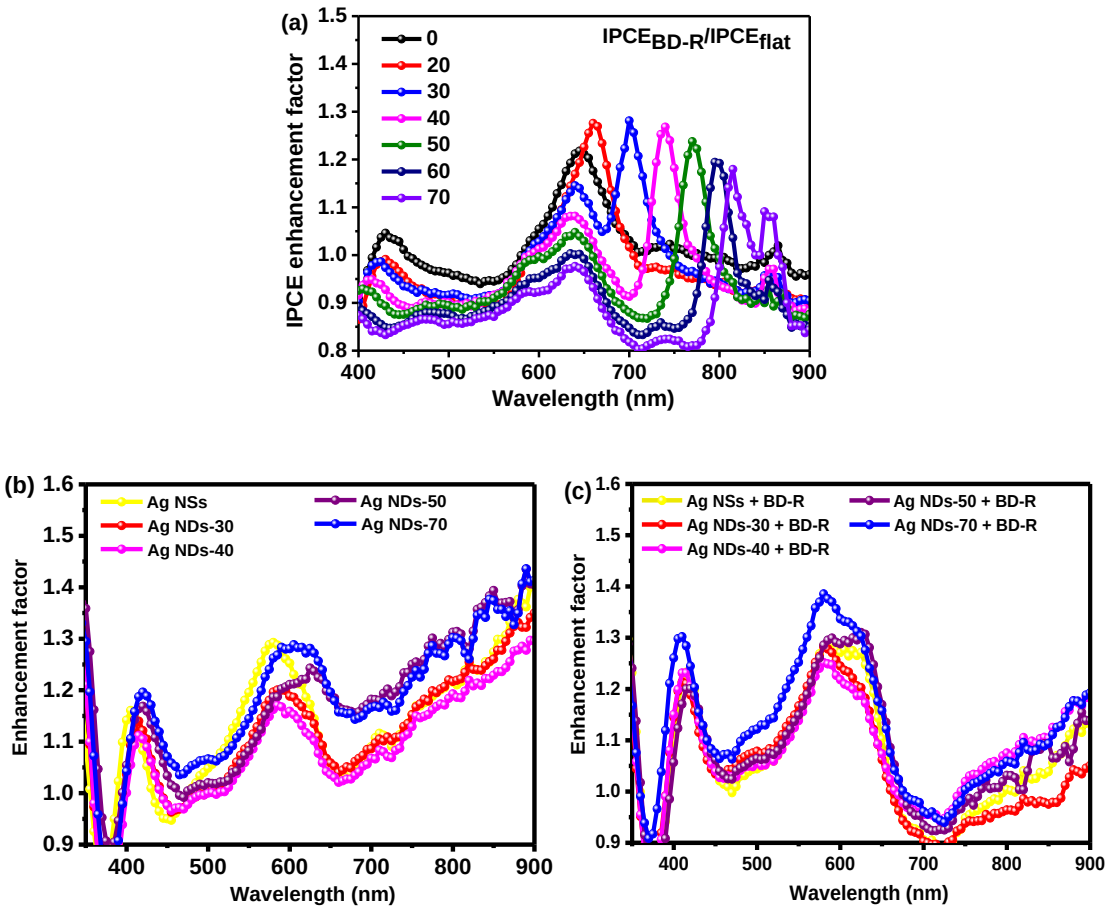

Figure 3.12 IPCE enhancement factor profiles of (a) the device imprinted with grating structure measured at different incident angles from 0º to 70º, (b) the devices incorporated with Ag NDs series, and (c) the devices incorporated with Ag NDs series and grating-imprinted structure of Al electrode.

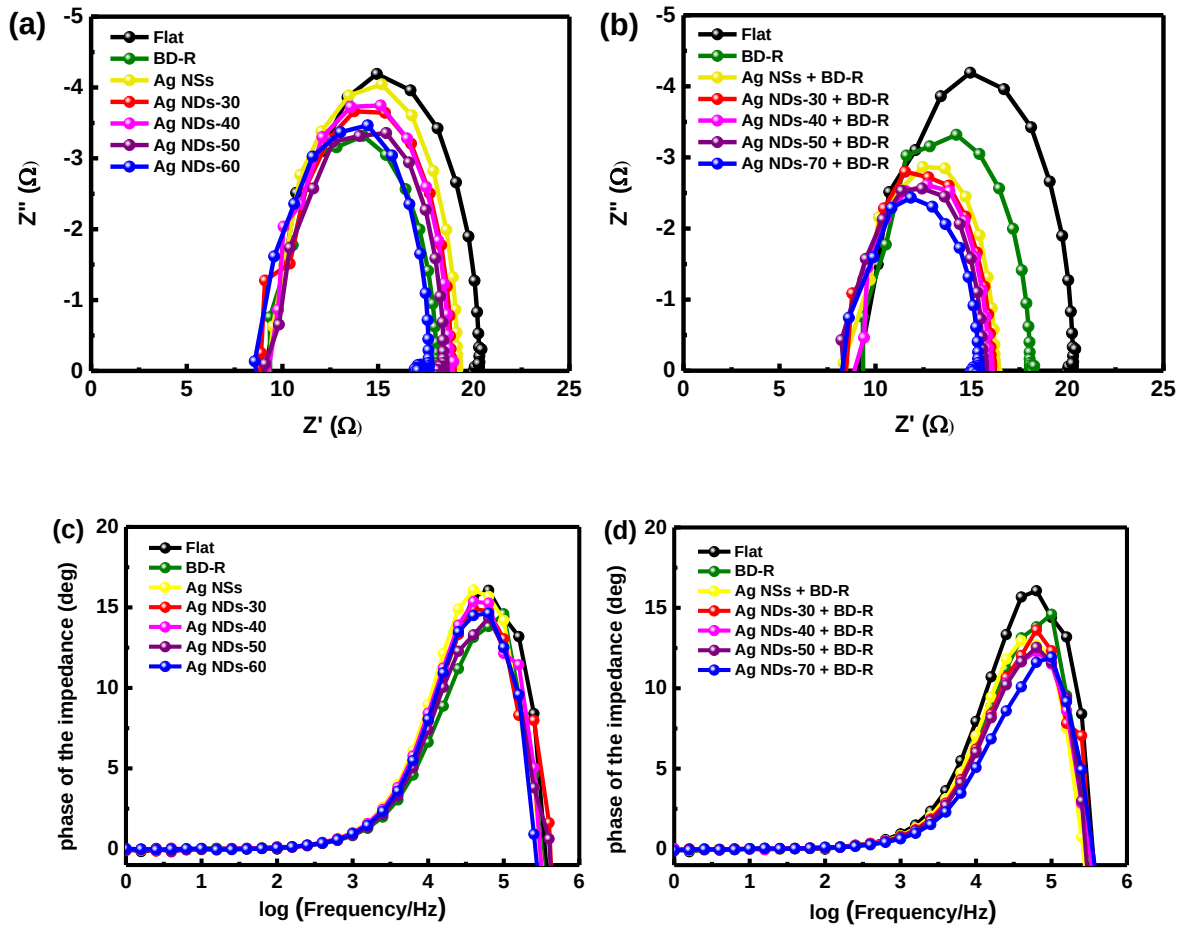

Figure 3.13 Nyquist plots of the devices: (a) incorporated with Ag NDs with different LSPR peaks and b) incorporated with Ag NDs with different LSPR peaks and imprinted Al grating. Bode phase plots: (c) corresponding to (a) and d) corresponding to (b).

The impedance spectra under illumination for studying resistance and charge transfer of the proposed devices exhibited semicircles of Nyquist plots as shown in Figure 3.13. Table 3.4 shows the summary of %PCE, J_{sc}, R_s and R_{ct} of the OPSCs. It can be seen that the impedance spectra typically display a large semicircle in the low frequency region. Moreover, noticeable drop in values of the real part (Z') and the imaginary part (Z") of the complex impedance along with an increase in the absorption wavelength of Ag NDs series, thus resulting in an decrease in the diameter of the charge transfer resistance semicircle. The diameter of the semicircle for the solar cell devices without Ag NDs series is much larger than those of the devices with Ag

NDs series and the diameter of the semicircle slightly decreases with increasing average Ag NDs diameter (figure 3.13 (a)). Moreover, the diameters of semicircles for devices incorporated with different Ag NDs are much larger than that of the devices with added Ag NDs and imprinted Al grating electrode (Figure 3.13(b)), indicating lowest charge transfer resistance. It be noted that the decreasing equivalent resistance by means of the introduction of Ag NDs series in PEDOT:PSS layer and Al grating can effectively decrease the series resistance of the devices, which is consistent with the enhanced photocurrent. The equivalent circuit of these OPSCs are described in the Figures 3.13(a) and 3.13(b) while represent series resistance (R_s) and charge transfer resistance (R_{ct}) values are summarized in Table 3.4. It was found that the with Al grating the R_s value decreased from 10.12 Ω to 9.37 Ω while incorporating Ag NDs series into HTL slightly decreased R_s value. With increasing the particles size of Ag NDs, the R_s value additionally dropped. The lowest R_s value was observed for the device with imprinted Al grating cathode and incorporated with Ag NDs series. Similarly, the device with Al grating also showed lower R_{ct} value than that of control device and with increasing the Ag NDs particles size, devices incorporated with Ag NDs series displayed a slight decrease in R_{ct} value. Device with Al grating and incorporated with Ag NDs series exhibited the R_{ct} value lower than those of devices with only Al grating or only incorporating Ag NDs series into HTL. This indicates that Al grating structure and/or Ag NDs series can improve the interfacial contact and charge transfer properties in OPSCs. Moreover, maximum frequency peaks of the Bode phase plots for OPSCs are shown in Figures 3.13(c) and 3.14(d). It can be seen that the device with only Al grating exhibits higher frequency peak compared to that of control device. The devices incorporated with only Ag NDs series display the frequency peaks slightly shifted to higher frequency with increasing particles size of Ag NDs. In the same way, frequency peaks of the device with Al grating and added with Ag NDs series slightly shifted regarding the increment of the Ag ND size. In addition, the electron lifetime or carrier lifetime (τ_{avr}), which is defined

as the average time it takes an excess minority carrier to recombine [46], can be calculated from the Bode phase plots and τ_{avr} values are summarized in Table 3.4. It was found that the average carrier lifetimes are not significantly different, suggesting that Al grating and Ag NDs in HTL might not significantly affect the carrier lifetime. Therefore, the performances of devices designed involving grating-coupled configuration and incorporating Ag NDs series into HTL is mainly improved by GCSPR, LSPR and light scattering.

Table 3.4 Power conversion efficiency (PCE), short-circuit current density (J_{sc}), average electron lifetime (τ_{avg}), maximum frequency (f_{max}), contact resistance (R_s) and charge transfer resistance (R_{ct}) of fabricated OPSCs.

Devices	**PCE (%)**	J_{sc} **(mA/cm$^{2)}$**	τ_{avg}	f_{max}	R_s	R_{ct}
Flat	2.98	6.42	4.80	33.17	10.12	10.13
Grating	3.16	6.99	5.00	31.85	9.37	8.69
Ag NPs	3.22	6.88	4.60	34.62	8.45	10.77
Ag NPs + grating	3.32	7.08	4.60	34.62	8.45	7.73
Ag NDs-30	3.27	7.10	4.60	34.62	8.34	10.66
Ag NDs-30+ grating	3.42	7.32	4.80	33.17	8.34	7.65
Ag NDs-40	3.29	7.05	4.80	33.17	8.23	10.64
Ag NDs-40+ grating	3.42	7.21	4.60	34.62	8.23	7.63
Ag NDs-50	3.33	7.05	4.80	33.17	8.22	10.35
Ag NDs-50+ grating	3.43	7.15	4.80	33.17	8.22	7.30
Ag NDs-70	3.37	6.97	4.80	33.17	8.13	10.20
Ag NDs-70+ grating	3.59	7.41	5.00	31.85	8.13	6.80

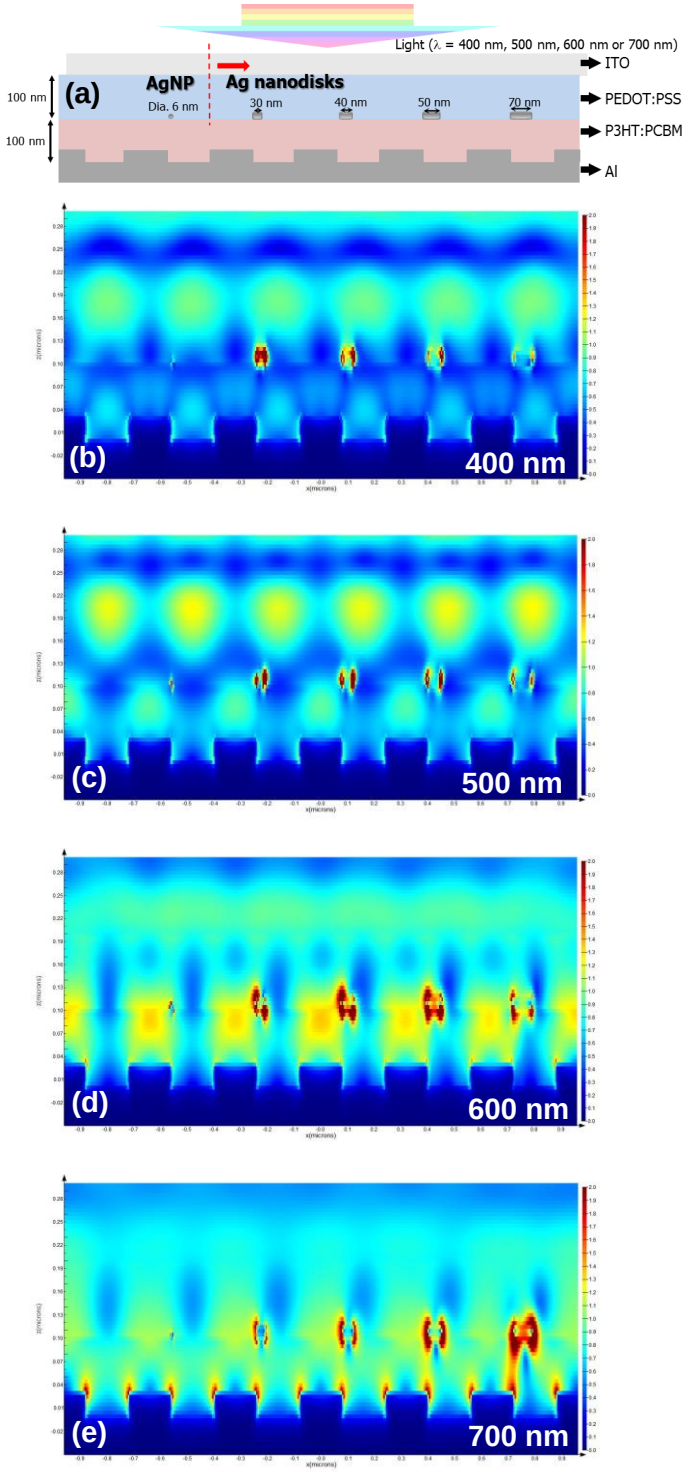

Figure 3.14 Schematic of the simulated structures (a) and electric field intensity maps of OPSCs with Ag NPs (diameter of 6 nm) and Ag NDs (diameter of 30, 40, 50 and 70 nm and thickness of 15 nm) in the PEDOT:PSS layer at illumination wavelengths of (b) 400 nm, (c) 500 nm, (d) 600 nm, and (e) 700 nm.

As shown in Figure 3.14, the FDTD simulation was employed to investigate the enhanced electric fields of Ag NSs and Ag NDs series incorporated into PEDOT:PSS layer by Al coated grating electrode. Model device structure for the FDTD simulation is shown in Figure 3.14(a). The device consists of Ag NPs with different sizes and Al grating cathode. At wavelength of 400 nm, the result from FDTD simulation clearly reveals that the Ag NDs-30 exhibit a higher electric field enhancement in comparison with those of other sizes, corresponding to the LSPR absorption spectra as illustrated in Figure 3.14(b). In case of incident light at wavelength of 500 nm (Figure 3.14(c)), it was found that the electric field at Ag NDs-30 and Ag NDs-40 can be enhanced while at 600 nm (Figure 3.14(d)) the electric field intensities of Ag NDs-40 and Ag NDs-50 are strongly enhanced, indicating the good interface of the active layer/Al-coated grating surface. Moreover, electric field at 700 nm (Figure 3.14(e)) exhibits a highest electric field intensity at Ag NDs-70 as compared to those of other sizes and shows a strongly enhanced the electric field intensity of the active layer/Al interface. This is attributed to induction of electric field surround both components. As a result, larger Ag NDs can enhance electric field intensity, which lead to increased absorption, scatting and trapping in the OPSCs, resulting in great light harvesting performance. Furthermore, it can be seen that the active layer/Al interface can enhance electric filed intensity in a range of 600-700 nm, which can lead to coupling the electric filed intensity of Ag NDs-50 and Ag NDs-70 resulted in higher photocurrent more than those of other sizes. The FDTD simulation result has a good agreement with the *J-V* curve and IPCE results.

3.5 CONCLUSIONS

In this research, we have successfully constructed the enhanced-OPSCs employing dual SPR phenomena originated from grating-coupled technique and addition of a series of plasmonic Ag NDs. Imprinting grating structure on the P3HT:PCBM active layer finished by Al electrode and/or incorporating Ag NDs into the PEDOT:PSS HTL, in turn, improved the

light harvesting as well as the power efficiency/device performances through induced local field enhancement surround additional plasmonic systems, better absorption property, better light trapping and light scattering within the devices. We achieved the best OPSC with configuration of Al grating/P3HT:PCBM/PEDOT:PSS-Ag NDs-70/ITO possessing a %PCE improvement of 20.47%. Moreover, cooperative plasmonic enhancement in OPSCs by combining grating structure and metal NP would be used for further development of other enhanced photovoltaics.

3.6 REFERENCES

[1] C-C. Chen, L. Dou, R. Zhu, C.-H. Chung, T.-B. Song, Y. B. Zheng, S. Hawks, G. Li, P. S. Weiss, Y. Yang, Visibly polymer solar cells produced by solution processing, *ACS Nano* **6[8]** (2012) 7185-7190.

[2] K. Yao, X. Xin, C. Chueh, K. Chen, Y. Xu, A. K. Jen, Enhanced light-harvesting by integrating synergetic microcavity and plasmonic effects for high-performance ITO-free flexible polymer solar cells, *Advanced Functional Materials* **25** (2015) 567-574.

[3] H. A. Atwater, A. Polman, Plasmonics for improved photovoltaic devices, *Nature Materials volume* **9** (2010) 205-213.

[4] J. D. Chen, C. Cui, Y. Q. Li, L. Zhou, Q. D. Ou, C. Li, Y. Li, J. X. Tang, Single-junction polymer solar cells exceeding 10% power conversion efficiency, *Advanced Materials* **27[6]** (2015) 1035-1041.

[5] Y. Yang, K. Mielczarek, M. Aryal, A. Zakhidov, W. Hu, Nanoimprinted polymer solar cell, *ACS Nano* **6[4]** (2012) 2877-2892.

[6] J. You, L. Dou, K. Zoshimura, T. Kato, K. Ohza, T. Moriarty, K. Emery, C.C. Chem, J. Gao, G. Li, Y. Yang, A polymer tandem solar cell with 10.6% power conversion efficiency, *Nature Communications* **4[1]** (2013) 1-10.

[7] A.M. Bagher, Introduction to organic solar cells, *Sustainable Energy* **2[3]** (2014) 85-90.

[8] L. Lu, Z. Luo, T. Xu, L. Yu, Cooperative plasmonic effect of Ag and Au nanoparticles on enhancing performance of polymer solar cells, *Nano Letters* **13[1]** (2013) 59-64.

[9] M. Yao, P. Shen, Y. Liu, B. Chen, W. Guo, S. Ruan, L. Shen, Performance Improvement of Polymer Solar Cells by Surface-EnergyInduced Dual Plasmon Resonance, *ACS Applied Materials & Interfaces* **8** (2016) 6183-6189.

[10] J. Cai, L. Qi, Recent advances in antireflective surfaces based on nanostructure arrays, *Materials Horizons* **2** (2015) 37-53.

[11] J. N. Munday, H. A. Atwater, Large integrated absorption enhancement in plasmonic solar cells by combining metallic gratings and antireflection coatings, *Nano Letters* **11[6]** (2011) 2195-2201.

[12] M. Sharma, P. R. Pudasaini, F. Ruiz-Zepeda, D. Elam, A. A. Ayon, Ultrathin, flexible organic-inorganic hybrid solar cells based on silicon nanowires and PEDOT:PSS, *ACS Applied Materials & Interfaces* **6[6]** (2014) 4356-4363.

[13] B-C. Chen, Y-S. Cheng, C. Gau, Y-C. Lee, Enhanced performance of polymer solar cells with imprinted nanostructures on the active layer, *Thin Solid Films* **564** (2014) 384-389.

[14] I. K. Ding, J. Zhu, W. Cai, S.-J. Moon, N. Cai, P. Wang, S. M. Zakeeruddin, M. Grätzel, M. L. Brongersma, Y. Cui, M. D. McGehee, Plasmonic Dye-Sensitized Solar Cells, *Advanced Energy Materials.* **1** (2011) 52-57.

[15] W. E. Sha, X. Li, W. C. Choy, Breaking the space charge limit in organic solar cells by a novel plasmonic-electrical concept, *Scientific Reports* **4[1]** (2014) 6236-6245.

[16] W. C. Choy, W. K. Chan, Y. Yuan, Recent advances in transition metal complexes and light-management engineering in organic optoelectronic devices, *Advanced Materials* **26[31]** (2014) 5368-5398.

[17] H Lan, Y Ding, Nanoimprint lithography, *Lithography* (2010) 457-494.

[18] H. Wu, J. Yang, S. Cao, L. Huang, L. Chen, Ordered organic nanostructures fabricated from anodic alumina oxide templates for organic bulk-heterojunction photovoltaics, *Macromolecular Chemistry and Physics* **215[7]** (2014) 584-596.

[19] W. M. Choi, O. O. Park, A soft-imprint technique for submicron-scale patterns using a PDMS mold, *Microelectronic Engineering* **73** (2004) 178-183.

[20] J. H. Lee, D. W. Kim, H. Jang, J. K. Choi, J. Geng, J. W. Jung, S. C. Yoon, H. T. Jung, Enhanced solar-cell efficiency in bulk-heterojunction polymer systems obtained by nanoimprinting with commercially available AAO membrane filters, *Small* **5[19]** (2009) 2139-2143.

[21] M. Aryal, F. Buyyukserin, K. Mielczarek, X. M. Zhao, J. Gao, A. Zakhidov, W.W. Hu, Imprinted large-scale high density polymer nanopillars for organic solar cells, *Journal of Vacuum Science & Technology B: Microelectronics and Nanometer Structures* **26[6]** (2008) 2562-2566.

[22] J. Hu, Y. Shirai, L. Han, Y. Wakayama, Template method for fabricating interdigitate p-n heterojunction for organic solar cell, *Nanoscale research letters* **7[469] (2012)** 1-5.

[23] A. J. Smith, C. Wang, D. Guo, C. Sun, J. Huang, Repurposing Blu-ray movie discs as quasi-random nanoimprinting templates for photon management, *Nature Communications* **5[5517]** (2015) 1-5.

[24] S. Nootchanat, A. Pangdam, R. Ishikawa, K. Wongraveeb, K. Shinbo, K. Kato, F. Kaneko, S. Ekgasitb, A. Baba, Grating-coupled surface plasmon resonance enhanced organic photovoltaic devices induced by Blu-ray disc recordable and Bluray disc grating structures, *Nanoscale* **9[15]** (2017) 4963-4971.

[25] K. Tvingstedt, N. K. Persson, O. Inganäs, Surface plasmon increase absorption in polymer photovoltaic cells, *Applied Physics Letters* **91** (2007) 113514(1)-113514(4).

[26] B. K. Singh, A. C. Hillier, Surface plasmon resonance imaging of biomolecular interactions on a grating-based sensor array, *Analytical Chemistry* **78** (2006) 2009-2018.

[27] W. Chomkitichai, H. Ninsonti, A. Baba, S. Phanichphant, K. Shinbo, K. Kato, F. Kaneko, Multiple plasmonic effect on photocurrent generation of metal-loaded titanium dioxide composite/dye films on gold grating surface, *Surface and Interface Analysis* **46[9]** (2014) 607-612.

[28] J. Homola, I. Koudela, S. S. Yee, Surface plasmon resonance sensors based on diffraction gratings and prism couplers: sensitivity comparison, *Sensor and Actuators B* **54[1-2]** (1999) 16-24.

[29] H. A. Atwater, A. Polman, Plasmonics for improved photovoltaic devices, *Nature Materials* **9[3]** (2010) 205-213.

[30] D. H. Wang, D. Y. Kim, K. W. Choi, J. H. Seo, S. H. Im, J. H. Park, O. O. Park, A. J. Heeger, Enhancement of donor-acceptor polymer bulk heterojunction solar cell power conversion efficiencies by addition of Au nanoparticles, *Angewandte Chemie International Edition* **50[24]** (2011) 5519-5523.

[31] J. L. Wu, F. C. Chen, Y. S. Hsiao, F. C. Chien, P. L. Chen, C. H. Kuo, M. H. Huang, C. S. Hsu, Surface plasmonic effects of metallic nanoparticles on the performance of polymer bulk heterojunction solar cells, *ACS Nano* **5[2]** (2011) 959-967.

[32] J. Yang, J. B. You, C. C. Chen, W. C. Hsu, H. R. Tan, X. W. Zhang, Z. R. Hong, Y. Yang, Plasmonic polymer tandem solar cell, *ACS Nano* **5[8]** (2011) 6210-6217.

[33] X. H. Li, W. C. H. Choy, L. J. Huo, F. X. Xie, W. E. I. Sha, B. F. Ding, X. Guo, Y. F. Li, J. H. Hou, J. B You, Y. Yang, Dual plasmonic nanostructures for high performance inverted organic solar cells, *Advanced Materials* **24[22] (2012)** 3046-3052.

[34] J. E. Millstone, S. J. Hurst, G. S. Métraux, J. I. Cutler, C. A. Mirkin, Colloidal gold and silver triangular nanoprisms, *Small* **5[6]** (2009) 646-664.

[35] M. Notarianni, K. Vernon, A. Chou, M. Aljada, J. Liu, N. Motta, Plasmonic effect of gold nanoparticles in organic solar cells, *Solar energy* **106** (2014) 23-37.

[36] A. Singh, A. Dey, D. Das, P. K. Iyer, Combined influence of plasmonic metal nanoparticle and dual cathode buffer layer for highly efficient rrP3HT: PCBM based bulk heterojunction solar cell**,** ***Journal of Materials Chemistry C*** **5** (2017) 6578-6587.

[37] F. Otieno, N. P. Shumbula, M. Airo, M. Mbuso, N. Moloto, R. M. Erasmus, A. Quandt, D. Wamwangi, Improved efficiency of organic solar cells using Au NPs incorporated into PEDOT:PSS buffer layer, *AIP Advances* **7** (2017) 085302(1)-085302(10).

[38] S.-W. Baek, J. Noh, C.-H. Lee, B. S. Kim, M.-K. Seo, J.-Y. Lee, Plasmonic forward scattering effect in organic solar cells: A powerful optical engineering method, *Scientific Reports* **3[1726]** (2013) 1-7.

[39] I. Pastoriza-Santos, L. M. Liz-Marzán, Colloidal silver nanoplates. State of the art and future challenges, *Journal of Materials Chemistry* **18[15]** (2008) 1724-1737.

[40] T. Parnklang, C. Lertvachirapaiboon, P. Pienpinijtham, K. Wongravee, C. Thammacharoen, S. Ekgasit, H_2O_2-triggered shape transformation of silver nanospheres to nanoprisms with controllable longitudinal LSPR wavelengths, *RSC Advances* **3[31]** (2013) 12886-12894.

[41] K. Wongravee, T. Parnklang, P. Pienpinijtham,C. Lertvachirapaiboon, Y. Ozaki, C. Thammacharoen, S. Ekgasit, Chemometric analysis of spectroscopic data on shape evolution of silver nanoparticles induced by hydrogen peroxide, *Physical Chemistry Chemical Physics* **15[12]** (2013) 4183-4189.

[42] Y. Yang, S. Feng, M. Li, Z. Wu, X. Fang, F. Wang, D. Geng, T. Yang, X. Li and B. Sun, Structure, optical absorption, and performance of organic solar cells improved by gold nanoparticles in buffer layers, *ACS Applied Materials & interfaces* **7[44]** (2015) 24430-24437.

[43] Y. M. Nama, J. Huh, W. H. Jo, Optimization of thickness and morphology of active layer for high performance of bulk-heterojunction organic solar cells, *Solar Energy Materials & Solar Cells* **94** (2010) 1118-1124.

[44] C. Lertvachirapaiboona, T. Maruyama, A. Baba, S. Ekgasit, K. Shinbo, K. Kato, Optical sensing platform for colorimetric determination of silver nanoprisms and its application for hydrogen peroxide and glucose detections using a mobile device camera, *Analytical Sciences* in press.

[45] Q. Fu, W. Sun, Mie theory for light scattering by a spherical particle in an absorbing medium. *Applied Optics* **40[9]** (2001) 1354-1361.

[46] R. L. Mattis, A. J. Baroody, Carrier lifetime measurement by the photoconductive decay method, *National Bureau of Standards Technical Note 736*, (1972) 1-52.

CHAPTER IV

CONCLUSIONS

This dissertation successfully demonstrates the fabrication of OPSCs with single and dual plasmonic systems. The fashion of the photovoltaic cell used in this study was of ITO/PEDOT:PSS/P3HT:PCBM/Al. Plasmonic metallic NPs and various kinds of micro/nanostructure patterns of finishing metal electrode including grating-imprinted patterns can enhance device properties such as PCE, J_{sc}, V_{oc}, and FF. In first research project, the influence of micro/nanopattern types of Al electrode on energy conversion performances of the proposed OPSCs was investigated. In developing and fabrication of the plasmonic OPSCs, creating each micro/nanostructure on active layer was carried out using the NIL technique, followed by coating with Al film as metal electrode, on which such structure was finally formed. For NIL process, each micro/nanostructure or each grating was completely transferred to the active layer of OPSCs using PDMS replicas. Improvement of the OPSC performances of the patterned devices was clearly observed. The improvement in the device performances is caused mainly by an increase in light absorption (light harvesting), which was attributed to the effects of either light scattering or GCSPR and both mechanisms. The patterns imprinted employing CD-R and BD-R gratings (1D grating) could provide the enhancement by both light scattering and GCSPR. Other imprinted patterns with nanodots and nanowells (2D gratings) revealed the improvement of light harvesting originated from only light scattering while the another 2D grating, namely honeycomb-imprinted structure, would offer both light scattering and GCSPR effects. The observable %PCEs are 2.49, 2.73, 3.09, 2.50, 2.65, and 2.58 for OPSCs with flat, CD-R-, BD-R-, nanodots-, nanowells-, and honeycomb-imprinted Al electrodes, respectively. As compared to the performance of bare OPSC, the best improvement of 24.09% was found with our OPSC imprinted with BD-R grating structure of Al electrode.

In second project, single plasmonic system with putting metallic NPs into HTL and dual plasmonic architecture based on HTL containing metallic NPs and grating-imprinted Al electrode were used in developing the plasmonic OPSCs with the same device configuration above. We successfully constructed the enhanced-OPSCs employing LSPR effect of added metal NPs in HTL or dual SPR phenomena originated from grating-coupled technique and additions of plasmonic NPs (Au NPs, Ag NSs, and a series of Ag NDs). Both plasmonic systems can actually enhance light harvesting over the broadband solar light for our developed OPSCs. It was found that dual plasmonic system which consists of LSPR and GCSPR effects of metal NPs and grating-nanoimprinted Al electrode works synergically, thus resulting in the noticeable enhancement of the photocurrent in the OPSCs. The observed improvement is attributed to the unique optical phenomena (LSPR, GCSPR and light scattering). Moreover, size of Ag NDs that would promote different LSPR excitations, light scatterings, and light absorptions, significantly affects %PCE and the enhancement of OPSCs. It was found that the observed %PCEs of dual plasmonic OPSCs are 3.32, 3.42, 3.42, 3.43, and 3.59 for incorporating with Ag NSs (6 nm), Ag NDs with average particle sizes of 30, 40, 50, and 70 nm, respectively. As compared to the performance of bare OPSC, the best improvement of 20.47% was achieved using Ag NDs with size of *ca*. 70 nm. Furthermore, cooperative plasmonic enhancement in OPSCs by combining grating structure and metal NPs in HTL could be used for further development of other photovoltaics.

SUGGESTIONS FOR FUTURE WORK

1. In order to obtain broadband light-harvesting, the advantages of the combination of plasmonic nanoparticles of Au NPs and Ag NDs should be investigated (i.e. loading concentration and position in OPSCs).

2. The cooperative effect of QDs and metallic nano/micro structures in OPSCs should be studied.

3. The our proposed plasmonic system should be applied to the construction of perovskite solar cells.

APPENDICES

APPENDIX A

SUPPORTING INFORMATION FOR CHAPTER II

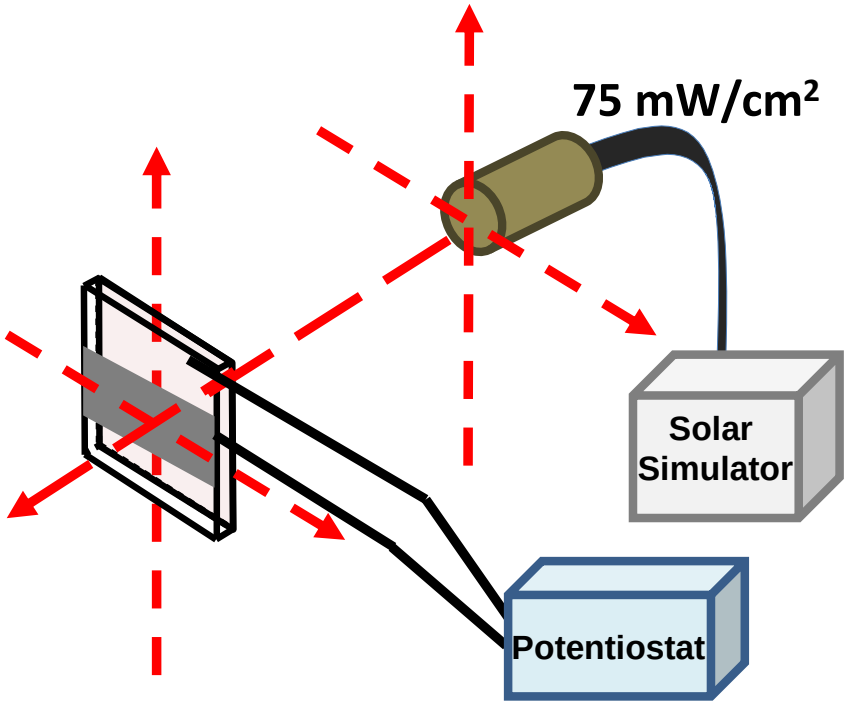

Figure A1.1 The photocurrent measurement apparatus.

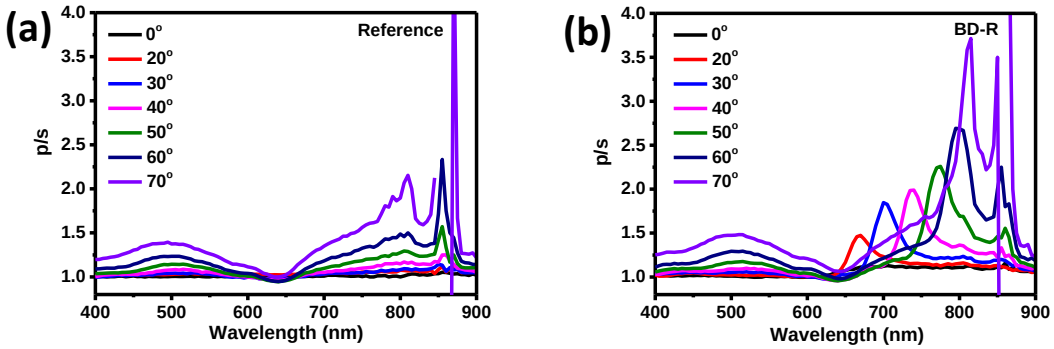

Figure A1.2 IPCE enhancement spectra p/s, the ratio between the IPCE with and without the SP excitation (p-polarization) for (a) flat and (b) BD-R grating devices.

APPENDIX B

SUPPORTING INFORMATION FOR CHAPTER III

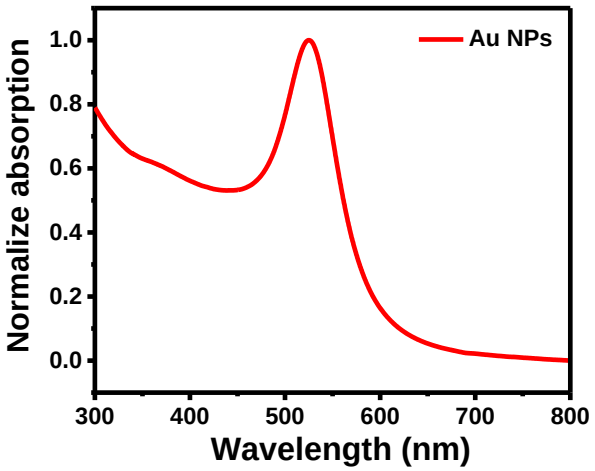

Figure B1.1 UV-visible absorption spectra of Ag NPs.

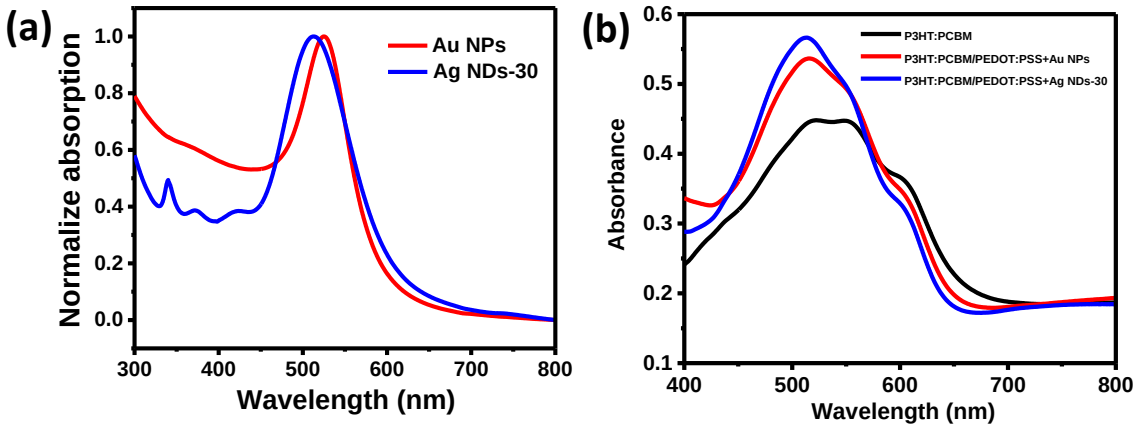

Figure B1.2 UV-visible absorption spectra of (a) Au NPs and Ag NDs-30 solutions and (b) ITO/PEDOT:PSS/P3HT:PCBM films without and with adding Au NPs or Ag NDs-30 in HTL.

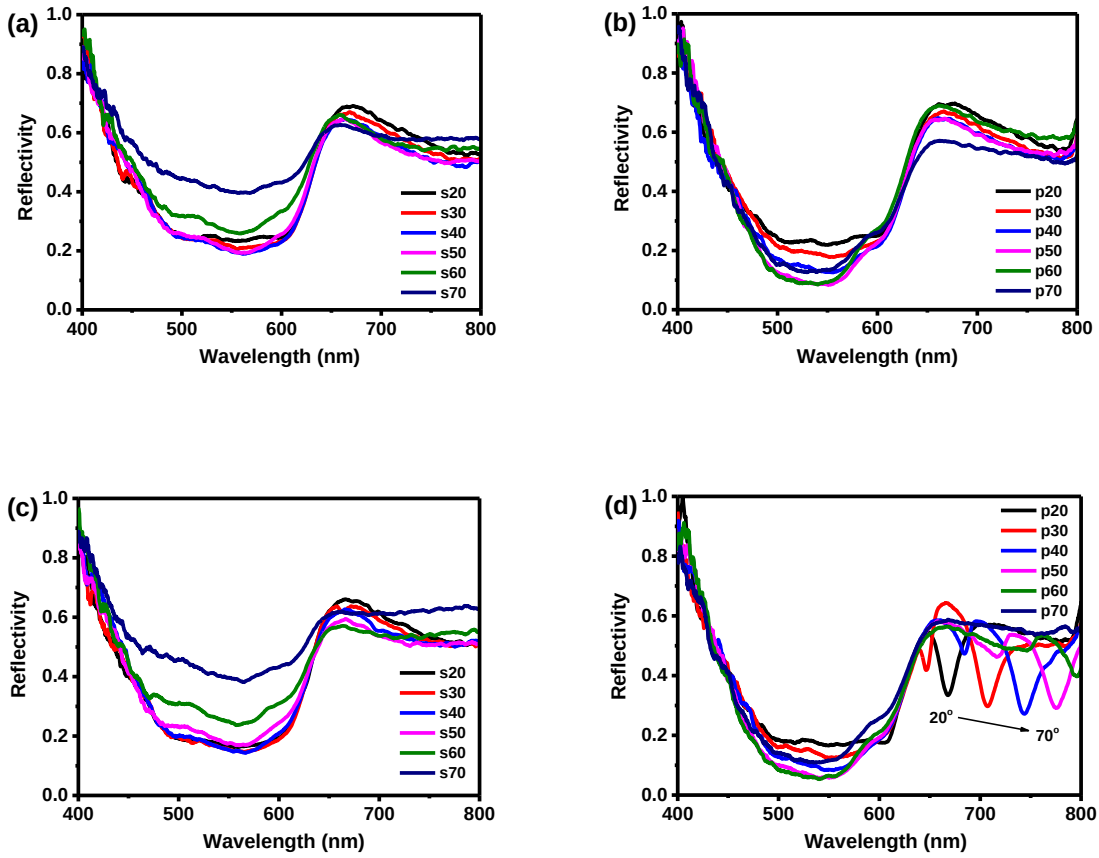

Figure B1.3 SPR reflectivity curves at various incident angles of 20°-70° for the solar cells based on flat Al electrode with Au NPs under incident (a) *s*-polarized and (b) *p*-polarized lights and based on Al grating with Au NDs under incident (c) *s*-polarized and (d) *p*-polarized lights.

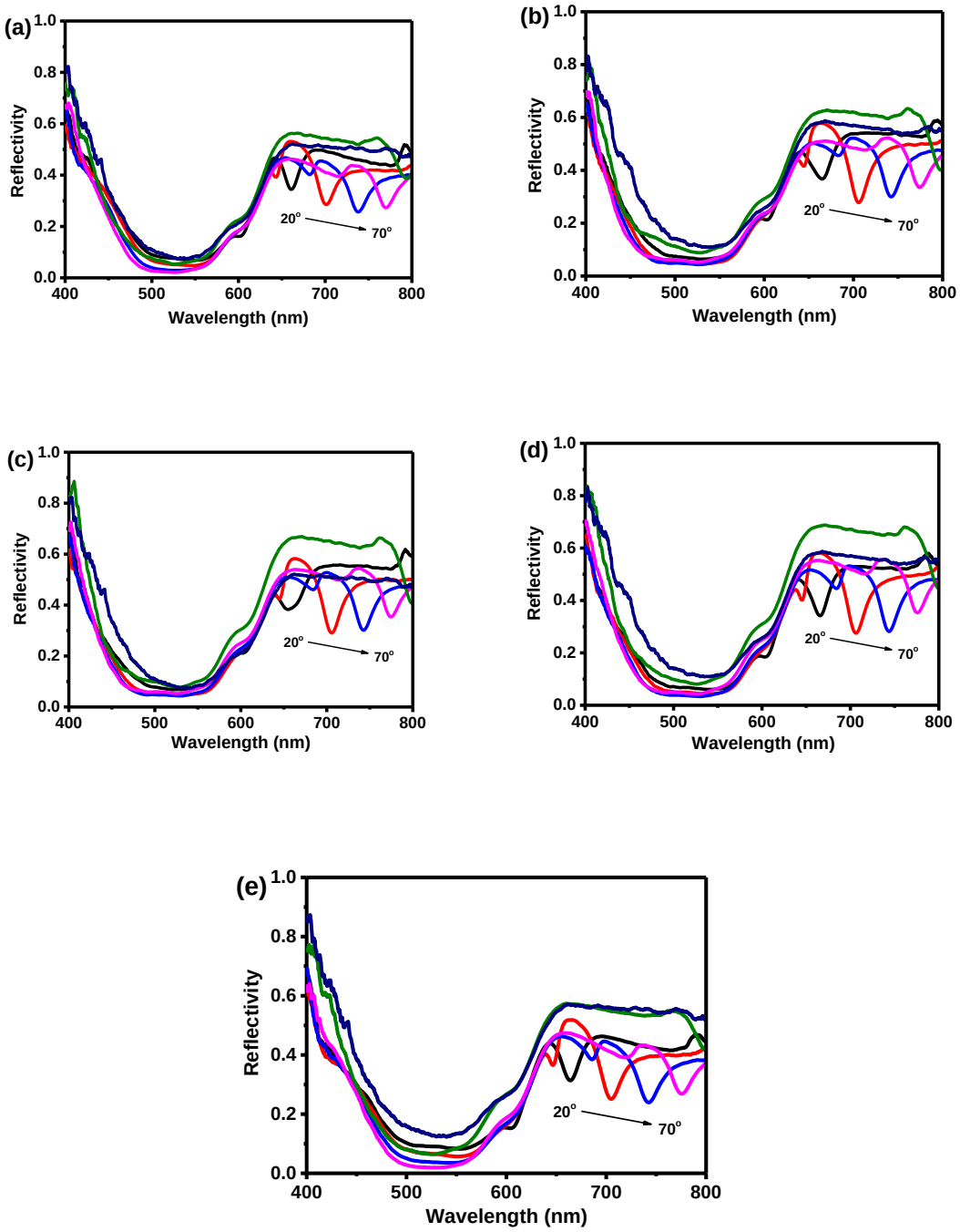

Figure B1.4 SPR reflectivity curves with *p*-polarization at various incident angles of 20°-70° for the solar cells with Al grating and (a) Ag NSs, (b) Ag NDs-30, (c) Ag NDs-40, (d) Ag-NDs-50, or (e) Ag NDs-40.

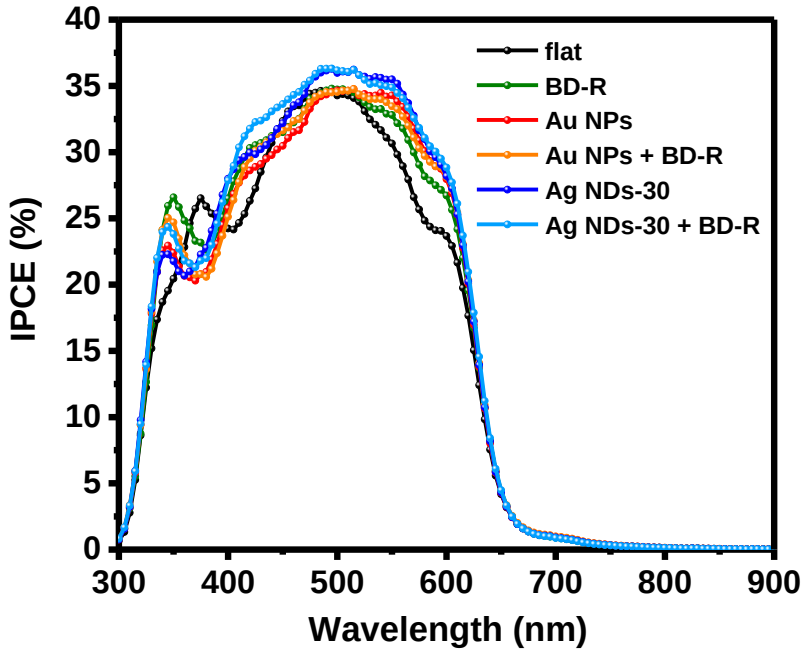

Figure B1.5 IPCE spectra of the devices incorporated with metallic nanoparticles (Au NPs and Ag NDs-30) and Al grating.

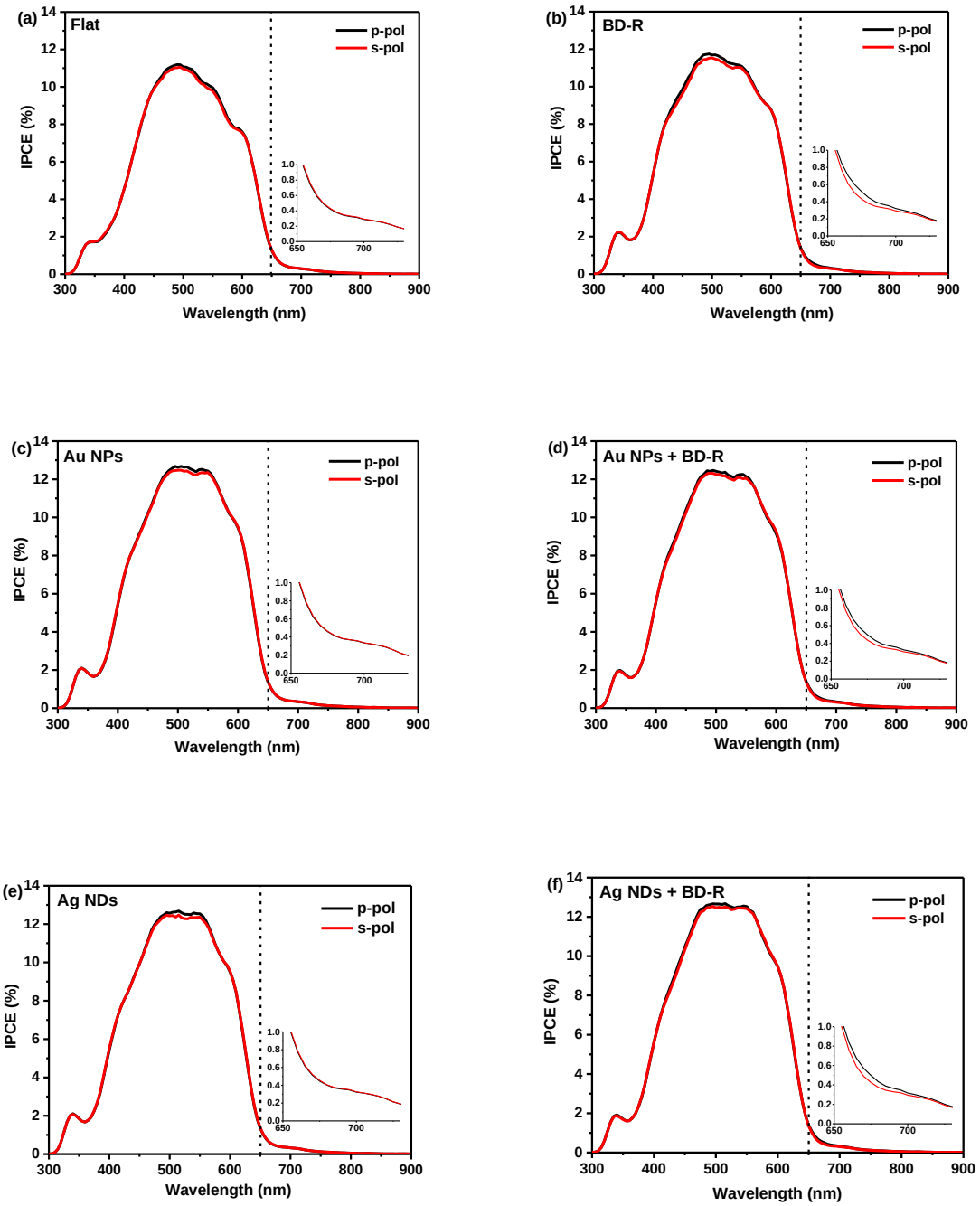

Figure B1.6 IPCE spectra with and without SP excitation measured at an incident angle of 20^{o} for the devices with (a) flat Al, (b) Al grating, (c) flat Al + Au NPs, (d) Al grating + Au NPs, (e) flat Al + Ag NDs, and (f) Al grating + Ag NDs.

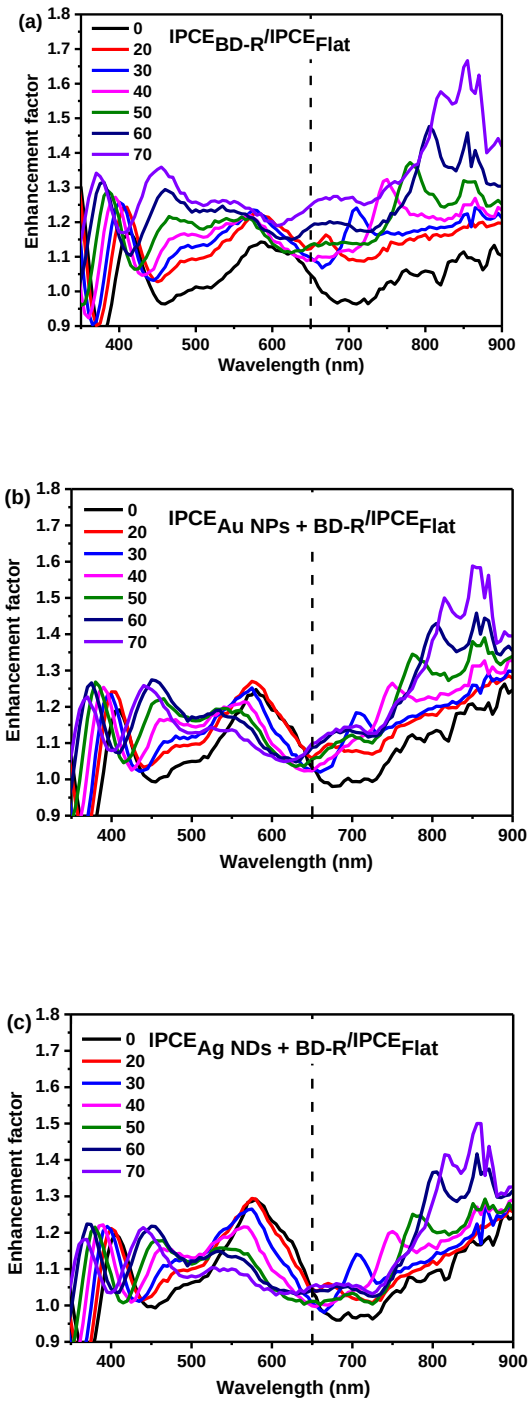

Figure B1.7 IPCE enhancement factor measured at incident angles from 0^{o} to 70^{o} for OPSCs with (a) Al grating, (b) Au NPs + Al grating, and (c) Ag ND + Al grating.

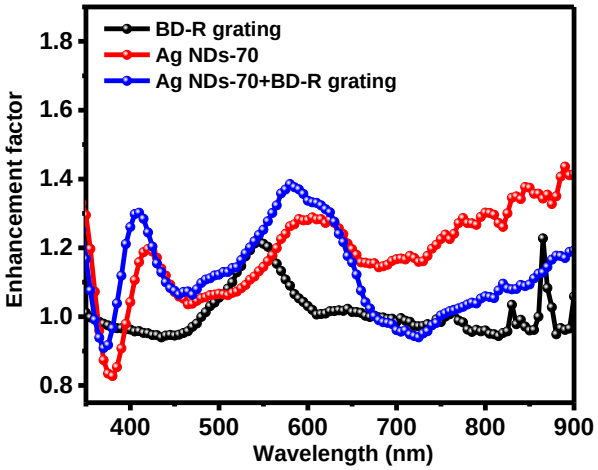

Figure B1.8 IPCE enhancement factor measured of incident angles at 0^{o} for OPSCs with Al grating, Au NDs-70 and Ag ND-70 + Al grating.

VITAE

NAME Miss Thitirat Putnin

DATE OF BIRTH June 13, 1989

SEX Female

ADDRESS 75, Phaongdam Road, Amphoe Mueang, Phitsanulok 65000,

THAILAND, Tel. +66-87-840-9417

E-mail; nooae_ka@hotmail.com, thitirat.pt091@gmail.com

EDUCATION

2008-2012 B.Sc. (Chemistry), Faculty of Science, Chiang Mai University, Thailand

Supervisor: Asst. Prof. Dr. Kontad Ounnunkad

2012-2014 M.Sc. (Chemistry), Faculty of Science, Chiang Mai University, Thailand

Supervisor: Asst. Prof. Dr. Winita Punyodom

2014-Present Ph.D. (Chemistry), Faculty of Science, Chiang Mai University, Thailand

Supervisor: Asst. Prof. Dr. Kontad Ounnunkad

2014-Present Ph.D. student in electrical engineering at Niigata University, Niigata, Japan

Supervisor: Assoc. Prof. Dr. Akira baba

SCHOLARSHIPS

2015-2016 Financial support from Graduate School of Science and Technology Niigata University, Japan (Double Degree Program, DDP)

2016 Financial support from Campus France of Cergy-pontoise University, France (France-co-Thai)

2017 Financial support from Campus France of Cergy-pontoise University, France (France-co-Thai)

2016-Present Full support from Thailand Graduate Institute of Science and Technology (TGIST)

PRESENTATIONS

2012 T. Putnin, K. Ounnunkad, W. Punyodom, P. Poungtong, N. Chandet, S. Phanichphant, S. Laiwruangrath, **"**Silver Nanoparticle-Eluting Wound Dressing for anti-infection", The 11th Pure and Applied Chemistry International Conference 2012 (PACCON 2012), January 11-13, 2012, Chiang Mai, Thailand.

2013 T. Putnin, K. Ounnunkad, W. Punyodom, P. Poungtong, N. Chandet, S. Phanichphant, S. Laiwruangrath, "Design and Development of Nano silver Gauzes for Anti-infection applications", The Technical Presentation and Innovation of Science Bachelor's Degree, February, 2013, Chiang Mai, Thailand.

2014 T. Putnin**,** R. Somsunan, P. Meepowpan, R. Molloy, W. Punyodom, **"**Synthesis and Characterization of Poly(L-lactide-*co*-glycolide) Using Liquid Tin(II) *n*-Butoxide Initiator", International Union of Pure and Applied Chemistry (MACRO 2014), July 6-11, 2014, Chiang Mai, Thailand.

2015 T. Putnin, R. Laocharoensuk, J. Jakmunee, K. Ounnunkad, "Label-Free Electrochemical Immunosensor Based on a Screen-Printed Carbon Electrode Modified with Poly(2-aminobenzylamine) Film for Detection of Human IgG", The 5th International Symposium on Organic and Inorganic Electronic Materials and Related Nanotechnologies (EM-NANO 2015), June 16-19, 2015, Niigata, Japan.

2015 T. Putnin, K. Ounnunkad, A. Baba, K. Shinbo, K. Kato, F. Kaneko**,** "Enhanced performances of organic polymer solar cells with imprinted grating structures on the active layer", The KJF International Conference on Organic Materials for Electronics and Photonics (KJF-ICOMEP 2015), September 6-9, 2015, Jeju, Korea.

2015 T. Putnin, K. Ounnunkad, C. Lertvachirapaiboon, K. Shinbo, K. Kato, F. Kaneko, A. Baba, "Enhanced Organic Thin Film Solar Cell Performance by Fabrication of Plasmonic Structures Using Nanoimprint Technique", The IEICE-IEEE-Shinetsu regional meeting, October 3, 2015, Niigata, Japan.

2015 T. Putnin, S. Nootchanat, K. Ounnunkad, C. Lertvachirapaiboon, K. Shinbo, K. Kato, F. Kaneko, A. Baba, "Effect of Nanostructured-Active Layers in Organic Polymer Thin Film Solar Cells", The 25th Annual meeting of Advanced

Materials Research as the Basis for the Technological Innovation (MRS-J 2015), December 8-10, 2015, Yokohama, Japan.

2015 T. Putnin, K. Ounnunkad, C. Lertvachirapaiboon, K. Shinbo, K. Kato, F. Kaneko, A. Baba, "Enhanced Performance of Polymer Solar Cells by Incorporating Metal NPs into PEDOT:PSS layer with Metallic Grating Top Electrode", The 63rd Japan Society of Applied Physics (JSAP 2016), March 19-22, 2015, Tokyo, Japan.

2016 T. Putnin, J. Jakmunee, P. Sangthong, K. Ounnunkad, R. Laocharoensuk, "Development of tagging NPs based on metal ions-adsorbed hollow porous gold nanoshells for signal amplification in immunosensing detection of cancer biomarkers", The 13th Asian Conference on Analytical Sciences (ASIANALYSIS XIII), December 8-11 2016, Chiang Mai, Thailand.

2018 T. Putnin, A. Ngamaroonchote, N. Wiriyakul, K. Ounnunkad, R. Laocharoensuk, "Highly sensitive simultaneous multiple electrochemical immunoassay based on poly(ethylenimine)-gold nanopaticles for determination of cancer biomarkers", The 17th Pure and Applied Chemistry International Conference 2018 (PACCON 2018), February 7-9, 2018, Hat Yai, Thailand.

AWARDS

2015 Young Researcher Presentation Award, in IEICE-IEEE-Shinetsu regional meeting 2015, Niigata, Japan.

PUBLICATIONS

2014 **"**Synthesis and Characterization of Poly(L-lactide-*co*-glycolide) Using Liquid Tin(II) *n*-Butoxide Initiator", **T. Putnin,** R. Somsunan, P. Meepowpan, W. Punyodom, *Proceeding of the International Union of Pure and Applied Chemistry* , 2014, *accepted*.

2017 "A sensitive electrochemical immunosensor based on poly(2-aminobenzylamine) film modified screen-printed carbon electrode for label-free detection of human immunoglobulin G", **T. Putnin**, W. Jumpathong, R. Laocharoensuk, J. Jakmunee, K. Ounnunkad, *Artificial Cells, Nanomedicine, and Biotechnology*, 2018, 46(5), 1042-105.

2018 "Poly(3,4-ethylenedioxythiophene/permethylated β-cyclodextrin) polypseudorotaxane and polyrotaxane: Synthesis, characterization and application as hole transporting materials in perovskite solar cells", **T. Putnin**,

H. Le, T-T. Bui, J. Jakmunee, K. Ounnunkad, S. Péralta, P-H. Aubert, F. Goubard, A. Farcas, *European Polymer Journal*, 2018, 105, 250-256.

2018 **“** Role of Cyano Substituents on Thiophene vinylene benzothiadiazole conjugated polymers and application as hole transporting materials in perovskite solar cells”, K. Mahesha, S. Karpagama, **T. Putnin**, H. Le, T-T. Bui, K. Ounnunkad, F. Goubardc, *Journal of Photochemistry and Photobiology A: Chemistry*, 2019, 371, 238-247.